question whether the expression of human APOBEC3B, DE, and F plays a critical role in HIV-1 restriction *in vivo*. The potential role of APOBEC3B in modulating HIV-1 replication *in vivo* is of particular interest because this protein is resistant to HIV-1 Vif-mediated degradation [20,22–24].

A polymorphic deletion of a 29.5-kb segment between *APOBEC3A* exon 5 and *APOBEC3B* exon 8 has been identified in human populations; this polymorphism causes the loss of the entire APOBEC3B coding region [25]. A particularly high frequency of *APOBEC3B* deletion has been found among Asians [25]. According to Kidd et al., the deletion allele is rare in Africans (1%) and Europeans (6%), more common in East Asians (36%) and Amerindians (58%), and almost fixed in Oceanians (93%) [25].

Two independent groups have reported contrasting findings concerning the effects of the *APOBEC3B* gene deletion on HIV-1 acquisition and disease progression [26,27]. An et al. determined that the deletion allele genotype correlated with a higher risk of HIV-1 infection, whereas a study conducted by Itaya et al. concluded that the deletion polymorphism had no effect on HIV-1 acquisition and the rate of disease progression to AIDS. An et al. included 4 patients with homozygous deletions of *APOBEC3B* in their HIV-1-seropositive cohorts of 656 European and 296 African-American individuals but no homozygotes for the deletion in their seronegative groups, which prevented a proper evaluation of the impact of the deletion polymorphism on HIV-1 acquisition and pathogenesis [26]. In contrast, the study conducted by Itaya et al. in Japan utilized inappropriate enrollment [27], because the enrolled patients were all hemophiliacs who had survived HIV-1 infection for at least 10 years prior to the study and the information for individuals who had progressed to AIDS and death before the enrollment date was excluded.

To examine the impact of the *APOBEC3B* deletion polymorphism on HIV-1 infection risk *in vivo*, this study enrolled a matched cohort in Japan and investigated the impact of *APOBEC3B* gene intact/deletion polymorphisms on HIV-1 susceptibility and pathogenesis. In addition, we analyzed the effects of different *APOBEC3B* genotypes on HIV-1 replication kinetics *in vitro*.

Materials and Methods

Sample Collection

A total of 248 Japanese HIV-1-positive men who have sex with men (MSM) who were patients at Nagoya Medical Center (n = 203) and Osaka Medical Center (n = 45) were enrolled in this study from November 2011 to February 2013. The control group comprised 207 Japanese HIV-1-negative MSM who were recruited at the Nagoya Lesbian & Gay Revolution Plus (NLGR+) festival in June 2012. The study protocol was approved by the ethics committees of Nagoya Medical Center (registration number 2011-430) and Osaka Medical Center. Written informed consent was obtained from all the participants. The control subjects recruited at the NLGR+ festival provided anonymous consent. To collect information regarding their sex, nationality, age, and sexuality, anonymous questionnaires collated with linked numbers were obtained.

Genotyping

The *APOBEC3B* intact (I) and deletion (D) alleles were genotyped using a previously reported polymerase chain reaction (PCR) method [26] with slight modifications. Of note, the "intact (I)" in this study is used for the "insertion" that originally reported by Kidd et al. [25]. Briefly, the primer sets for amplifying the Deletion and Insertion 2 fragments were the same as those previously described [26], although one additional set of primers for the Insertion 1 fragement was replaced by the two following oligonucleotide primers: Insertion3_F: 5′-GAGTG-GAAGCGCCTCCTC-3′ and Insertion3_R: 5′-CTCCTGGCCAGCCTAGC-3′. The QIAamp DNA Blood Mini Kit (Qiagen, Valencia, USA) was used according to the manufacturer's protocol to extract genomic DNA from whole blood (patients) or from buccal mucosa (controls).

Analysis of Viral Replication Capacity and Infectivity

Peripheral blood mononuclear cells (PBMCs) were isolated from fresh blood samples from different HIV-1-negative donors with the I/I and D/D *APOBEC3B* genotypes (n = 5 for each) using Ficoll-Hypaque density gradient centrifugation (Pharmacia, Uppsala, Sweden). The PBMCs were then subjected to negative selection with the MACS CD4 T Cell Isolation Kit (Miltenyi Biotec, Cologne, Germany) to purify primary $CD4^+$ T cells. The cells were activated with 1 μg/ml of phytohemagglutinin (PHA) (Pharmacia) for 72 hours, infected with HIV-1 NL4-3 for 24 hours with a multiplicity of infection (MOI) of 0.01, washed twice, and maintained in RPMI-1640 medium with 20% fetal bovine serum (FBS), penicillin (50 U/ml)/streptomycin (50 μg/ml) (Invitrogen, Carlsbad, USA), and 20 U/ml interleukin-2 (IL-2) (Roche Applied Science, Mannheim, Germany). The culture supernatants were assayed for the p24 antigen using the HIV-1 p24 Antigen Assay Kit (Coulter Corporation, Fullerton, USA) on the day of infection and on days 2, 4, 6, 8, 10, and 13 after infection. To analyze the viral infectivity of the infected PBMCs, culture supernatants were harvested six days post-infection and inoculated into TZM-bl cells [29] in black 96-well plates. The viral infectivity was assessed 48 hours post-infection by detecting β-galactosidase activity using the Galacto-Star System (Applied Biosystems, Foster City, USA).

Quantification of APOBEC3 mRNA

To analyze the mRNA expression levels of members of the APOBEC3 family, unstimulated $CD4^+$ cells from three different genotyped subjects were prepared for RNA isolation. The induction rates of mRNA transcription for APOBEC3A or APOBEC3G were analyzed using monocyte-derived macrophages (MDMs). Briefly, monocytes were isolated from PBMCs from each genotyped healthy donor using CD14 MicroBeads (Miltenyi Biotec). The enriched $CD14^+$ cells were plated at a cell density of 1×10^6/ml in 12-well plates in RPMI-1640 medium (Sigma, St. Louis, USA) with penicillin (50 U/ml)/streptomycin (50 μg/ml) for three hours, followed by the addition of 10% FBS and 10 ng/ml macrophage colony stimulating factor (M-CSF) (Peprotech, Rocky Hill, USA). Adherent cells were cultured for eight days to facilitate their differentiation into MDMs. Differentiated MDMs either received no stimulation or were stimulated with 100 U/ml of recombinant human interferon (IFN)-α (Sigma) for six hours and were then lysed for RNA isolation. As previously described [14.30], total RNA isolated using the QIAamp RNA Blood Mini Kit (Qiagen) was used to synthesize cDNA with the SuperScript III First-Strand Synthesis System (Invitrogen) using random hexamers. The cDNA levels were quantified using real-time PCR in a Thermal Cycler Dice Real Time System (TP800) (Takara Bio, Shiga, Japan). The real-time PCR was employed to analyze the levels of APOBEC3, β-actin, and GAPDH mRNA, and the assays were performed according to the manufacturer's protocol using SYBR Premix DimerEraser (Takara Bio). The primer sets for the real-time PCR were purchased from FASMAC Co., Ltd. (Atsugi, Japan) and the oligonucleotide sequences are

shown in Table S1. The gene expression levels were calculated using the ΔΔCt (Ct; cycle threshold) and are presented as the ratio of APOBEC3 mRNA to β-actin or GAPDH mRNA.

Statistical Analysis

The relationships between *APOBEC3B* genotype and baseline characteristics were assessed using the Fisher exact test for categorical variables. The Mann-Whitney *U*-test was used for continuous variables. All the statistical analyses were performed with the statistical software EZR (Saitama Medical Center, Jichi Medical University), which is a graphical user interface for R (The R Foundation for Statistical Computing, version 2.13.0). More specifically, this software is a version of R commander (version 1.6–3) modified to add statistical functions that are frequently used in biostatistics [31]. All the p values were two-tailed. The effects of *APOBEC3B* gene deletion on the disease progression of HIV-1 were evaluated based on the CD4+ T cell counts and log10 HIV-1 viral load (RNA copy number/ml) at more than two time points before the start of antiretroviral therapy (ART). Patients whose $CD4^+$ T cell counts and HIV-1 viral loads were measured at fewer than two time points were excluded from the statistical analyses of these factors. Other related infectious diseases were identified in the patients using the following definitions. If the rapid plasma reagin test and/or the *Treponema pallidum* latex agglutination (TPHA) test were positive, the patient was considered positive for syphilis. Patients were considered hepatitis B virus (HBV)-positive if either hepatitis B surface antigen (HBsAg) or hepatitis B core antibody (HBcAb) was present. In addition, patients were considered hepatitis C virus (HCV) carriers if they tested positive for HCV antibodies.

Results

APOBEC3B Genotype Frequencies in the Cohorts

The demographics of the HIV-1-positive and HIV-1-negative cohorts are shown in Table 1. A total of 248 HIV-1-infected Japanese MSM patients and 207 uninfected Japanese MSM were enrolled and analyzed in this study. To conduct a matched cohort study, all the participants were recruited from Nagoya and Osaka in the central area of Japan. First, a comparative analysis of the *APOBEC3B* genotype among the participants indicated that there were no significant differences in *APOBEC3B* genotype frequency between the HIV-1-positive (D/D 7.7%, I/D 44.0%, and I/I 48.4%) and HIV-1-negative (D/D 8.7%, I/D 39.6%, and I/I 51.7%) cohorts ($p = 0.66$) (Table 1). A comparison of the distributions of the *APOBEC3B* deletion allele in the HIV-1-positive and HIV-1-negative cohorts revealed that the D allele occurred in the HIV-1-positive (29.6%) and HIV-1-negative subjects (28.5%) at comparable rates ($p = 0.71$). We also analyzed the cDNA sequences of *APOBEC3B* I allele isolated from the Japanese healthy donors with the I/I or I/D genotypes (Table S1). There was one variant (rs#2076109): K62 (allele frequency, or $AF = 0.4$) (E62 as the reference) although we could not detect any other variants changing the amino acid sequences within the 15 alleles. According to the 1000 Genome database, the variant ($AF = 0.373$) appears globally distributed but not limited in Japan or Asia. In addition, we tested the antiviral effect of APOBEC3B E62 and the variant with an overexpression system using 293T cells (Figure S1). The results demonstrated that the E62 variant had equivalent antiviral activity to APOBEC3B K62 *in vitro*. These data suggest that the I alleles in our Japanese cohorts are not strongly biased in terms of genetic and functional features.

Next, we analyzed the HIV-1-positive individuals for the prevalence of HBV, HCV, and syphilis, as well as for HIV-1 disease progression at a minimum of two time points before the commencement of ART. The prevalence of each infectious disease is presented in Table 2. The frequencies of the three *APOBEC3B* genotypes (D/D 7.6%, I/D 45.4%, and I/I 47.0%) among the 132 HBV-positive patients were not significantly different from those of the 94 HBV-negative individuals (D/D 9.6%, I/D 41.5%, and I/I 48.9%) ($p = 0.69$). In addition, the *APOBEC3B* genotype distributions did not differ significantly between the HCV-positive and HCV-negative patients ($p = 1.00$) or between the syphilis-positive and syphilis-negative patients ($p = 0.62$) (Table 2).

We also assessed the rates of both $CD4^+$ T cell decline and plasma viral load increase at different time points after the first patient visit to the hospital prior to ART treatment. As shown in Figure 1, the changes in the $CD4^+$ T cell counts (cells/μl/day) and viral loads (log_{10} copies/ml/day) did not differ significantly according to *APOBEC3B* genotype (CD4: $p = 0.054$; viral load: $p = 0.96$). The data from the 46 patients (D/D 6.5%, I/D 41.3%, and I/I 52.2%) who began ART before the second measurement of the $CD4^+$ T cells and viral loads were excluded from the analysis. Of these 46 patients, 32 (D/D 3.1%, I/D 50.0%, and I/I 46.9%) began ART shortly after their first hospital visit due to AIDS onset; this decision was based on the domestic clinical guidelines of the Ministry of Health, Labor, and Welfare of Japan. There were no significant differences in the proportions of the *APOBEC3B* genotypes between the patients with $CD4^+$ T cell count and viral load data from at least two time points and the 46 patients without complete data ($p = 0.91$). Detailed demographic information on the HIV-1 (+) patients is shown in Table 3. Moreover, we analyzed the non-ART periods from the first diagnosis through the ART introduction and set two groups: longer and shorter than median days from diagnosis to ART. As the genotype frequencies were compared (Table 4), the results showed no significant difference in the *APOBEC3B* genotype between the two groups ($p = 0.96$).

Moreover, we performed deep sequencing of the HIV-1 proviral DNAs that were isolated from the I/I, I/D or D/D patients' PBMCs, and then analyzed the hypermutation rates on APOBEC3-prefered dinucleotide sequences: GG>AG and GA>AA mutations. The results showed that the hypermutation frequencies vary among different individuals although the levels of GA>AA hypermutation relative to the GG>AG are comparable among the three *APOBEC3B* genotypes (Figure S2). The data suggest that the APOBEC3B is not likely a major contributor to introduce hypermutations on the proviral DNAs in HIV-1(+) patients' PBMCs.

The Effects of *APOBEC3B* Genotype on Other APOBEC3 Expression Profiles

To assess whether the *APOBEC3B* gene deletion altered the expression of the other proximal *APOBEC3* genes, we compared mRNA expression profiles in fresh, unstimulated primary $CD4^+$ cells of each *APOBEC3B* genotype: D/D, I/D, and I/I. As shown in Figure 2A, the mRNA expression levels of APOBEC3A, which is the *APOBEC3* family member located closest to the *APOBEC3B* gene, were not significantly different between the I/I and D/D genotype groups ($p = 0.63$), although the levels would likely vary considerably among individuals. As expected, APOBEC3B mRNA expression levels were not detected in the D/D subjects (Figure 2A). The APOBEC3B mRNA levels in the I/D subjects were somewhat lower than in the I/I subjects, although this difference was not statistically significant (Figure 2A, $p = 0.12$). Moreover, the relative levels of APOBEC3C, DE, F, G, and H mRNA were comparable among the I/I, I/D, and D/D subjects (Figure 2A). We also analyzed APOBEC3B mRNA levels in

Table 1. *APOBEC3B* genotype frequency in HIV-1-positive patients and HIV-1-negative controls.

	HIV-1		
	Negative (%)	**Positive (%)**	**p[a]**
Genotype			
D/D	18/207 (8.7)	19/248 (7.7)	0.66
I/D	82/207 (39.6)	109/248 (44.0)	
I/I	107/207 (51.7)	120/248 (48.4)	
Allele			
D	118/414 (28.5)	147/496 (29.6)	0.71
I	296/414 (71.5)	349/496 (70.4)	

[a]Determined using the Fischer exact test.
doi:10.1371/journal.pone.0092861.t001

PBMCs isolated from healthy donors and HIV-1 seropositive patients with or without the ART. Similar to the pattern of APOBEC3B mRNA levels in the CD4+ T cells of three genotyped subjects (Figure 2A), the mRNA expression is slightly lower in the I/D genotyped PBMCs than in the I/I whereas no detectable level of APOBEC3B mRNA in the D/D PBMCs (Figure S3). The different expression levels between the I/D and I/I PBMCs were not statistically significant (Figure S3). Moreover, comparative analysis showed that the APOBEC3B mRNA level of each I/I or I/D genotype appears relatively higher in the HIV-1 (+) patients, regardless the ART-treatment, than in the uninfected donors. However, the difference was not statistically significant (Figure S3).

In the *APOBEC3B* D allele, the APOBEC3A mRNA contains a 3′-untranslated region of APOBEC3B's and is subject to the upstream regulatory elements of the *APOBEC3A*. Thus, we further assessed whether the degrees to which APOBEC3A and APOBEC3G mRNA expression was stimulated by IFN-α in MDMs differed between the *APOBEC3B* I/I and D/D genotypes. The APOBEC3G mRNA expression was used as a control because the gene is distal to the *APOBEC3B* loci on the genome. As shown in Figure 2B, IFN-α stimulation resulted in APOBEC3A mRNA increases in the I/I and D/D MDMs of 1,999±1,190-fold and 1,251±264-fold, respectively. The APOBEC3G mRNA levels increased upon IFN-α stimulation by 28.6±41.8-fold (I/I) and 38.9±18.0-fold (D/D). A comparison of the mRNA expression magnitudes between the two homozygous *APOBEC3B* genotypes revealed no significant differences ($p = 0.4$ and $p = 0.4$ for APOBEC3A and APOBEC3G, respectively).

The Effects of *APOBEC3B* Genotype on HIV-1 Susceptibility *in Vitro*

We further analyzed the viral replication kinetics in primary PBMCs isolated from D/D or I/I donors. At an MOI of 0.01, the efficiency of HIV-1 replication was comparable between the D/D and I/I genotypes (Figure 3A). The p24 antigen levels in the culture supernatant from the I/I and D/D PBMCs were $8.7 \pm 3.0 \times 10^5$ pg/ml and $1.3 \pm 0.2 \times 10^6$ pg/ml, respectively, on day 8 ($p = 0.31$) and $8.4 \pm 0.2 \times 10^5$ pg/ml and $1.3 \pm 0.3 \times 10^6$ pg/ml, respectively, on day 6 ($p = 0.13$). At the peak of infection (day 6), the virus-containing supernatants derived from D/D and I/I PBMCs exhibited comparable levels of infectivity ($p = 0.86$) (Figure 3B). These data suggest that the different *APOBEC3B* deletion genotypes are not associated with significantly different levels of HIV-1 susceptibility *in vitro*.

Table 2. *APOBEC3B* genotype frequency and clinical parameters in HIV-1-positive patients.

	***APOBEC3B* genotype**			
	D/D (%)	**I/D (%)**	**I/I (%)**	**p[a]**
HBV				
Positive	10/132 (7.6)	60/132 (45.4)	62/132 (47.0)	0.69
Negative	9/94 (9.6)	39/94 (41.5)	46/94 (48.9)	
Unknown	0/22 (0)	10/22 (45.5)	12/22 (54.5)	
HCV				
Positive	0/7 (0)	3/7 (42.9)	4/7 (57.1)	1.00
Negative	19/241(7.9)	106/241 (44.0)	116/241 (48.1)	
Syphilis				
Positive	9/116 (7.8)	47/116 (40.5)	60/116 (51.7)	0.62
Negative	10/131 (7.6)	61/131 (46.6)	60/131 (45.8)	
Unknown	0/1 (0)	1/1 (100)	0/1(0)	

[a]Determined using the Fischer exact test.
doi:10.1371/journal.pone.0092861.t002

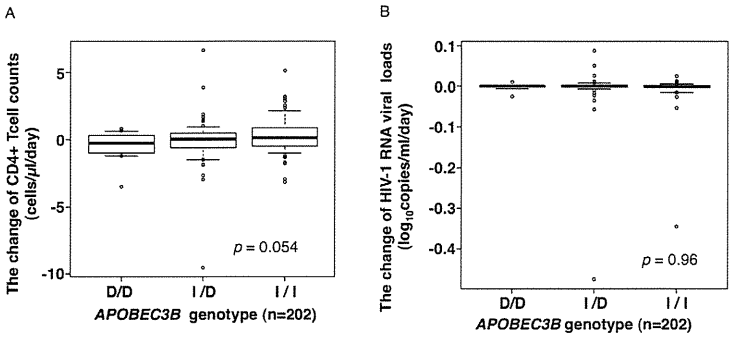

Figure 1. Analysis of effects of genotype on parameters of HIV disease progression in the HIV-1-infected cohort. (A) Changes in $CD4^+$ T cell counts (cells/μl/day) (n = 202). (B) Changes in HIV-1 RNA levels (log_{10} copies/ml/day) in plasma (n = 202). The box plots show data between the 25th and 75th percentiles with central horizontal lines representing the median, and with whiskers showing the 10th and 90th percentiles. The open circles represent outliers with data >1.5-fold of the interquartile range. All the p values were determined using the Kruskal-Wallis test.
doi:10.1371/journal.pone.0092861.g001

Discussion

There is only limited information about the roles played by APOBEC3 family members *in vivo*, with the exception of APOBEC3G. Previously, two independent groups reported conflicting conclusions regarding the impact of the *APOBEC3B* gene deletion on human HIV-1 infection *in vivo*, and this issue remains unclear [26,27]. Therefore, to determine the effects of different *APOBEC3B* genotypes on HIV-1 infection *in vivo* and *in vitro*, we investigated the frequencies of intact and deletion polymorphisms of the *APOBEC3B* gene in a matched cohort in Japan.

The comparison of *APOBEC3B* genotypes in HIV-1-infected patients and HIV-1-negative controls revealed similar *APOBEC3B* genotype distributions in the two groups: D/D 7.7%, I/D 44.0%, and I/I 48.4% in the infected cohort versus D/D 8.7%, I/D 39.6%, and I/I 51.7% in the uninfected cohort (p = 0.66). In addition, no significant associations between the *APOBEC3B* genotype and the subclinical parameters of disease progression were observed among the HIV-1-positive patients. We also found no differences between the mRNA expression profiles of other APOBEC3 family members in PBMCs. Furthermore, the IFN-α-stimulated mRNA induction rates for APOBEC3A and APOBEC3G in MDMs did not differ between the D/D and I/I genotypes. Moreover, the HIV-1 susceptibility levels in PBMCs were comparable between the two genotypes. Considered together, our findings suggest that the loss of APOBEC3B is not significantly associated with HIV-1 acquisition and pathogenesis *in vivo* and with HIV-1 susceptibility *in vitro*, which fully supports the results of the cohort study conducted by Itaya et al [27].

There are two possible explanations for the lack of APOBEC3B involvement in HIV-1 restriction. First, the APOBEC3B protein cannot be incorporated into viral cores. Efficient HIV-1 restriction requires that APOBEC3 family proteins are packaged into virions through associations with viral and/or nonviral RNA [1,2,28–30] and that the proteins are localized to the plasma membrane in virus-producing cells [31]. APOBEC3G colocalizes with HIV-1 RNA and cellular RNA in P bodies [32] and are dispersed throughout the cytoplasm that facilitate interactions with HIV-1 Gag proteins and their incorporation into nascent virions [1,2]. In contrast, APOBEC3B predominantly localizes to the nucleus [20,21,33], which may prevent its incorporation into virions.

The second possible explanation is that the low expression level of APOBEC3B in PBMCs [22,34,35] is insufficient to block HIV-

Table 3. Demographics of the cohorts.

	HIV-1 Negative (n = 207)	HIV-1 Positive (n = 248)
Age (years), median [IQR][a]	33 [26–39]	40 [36–51]
Year of diagnosis, median [IQR] [a]	NA[b]	2008 [2005–2010]
ART naïve at entry, n (%)	NA[b]	20 (8%)
$CD4^+$ cell count at entry (cells/mm^3), median [IQR] [a]	NA[b]	451 [294–534]
HIV-1 viral load at entry (copies/mL), median [IQR] [a]	NA[b]	61 [<40–410]
History of AIDS, n (%)	NA[b]	32 (13%)
Days from diagnosis to entry, median [IQR] [a]	NA[b]	1470 [539–2256]
Observation periods for disease progression (days), median [IQR] [a]	NA[b]	56 [28–88]
Days from diagnosis to ART, median [IQR] [a]	NA[b]	88 [38–599]

[a]IQR denotes interquartile range.
[b]NA, Not applicable.
doi:10.1371/journal.pone.0092861.t003

Table 4. *APOBEC3B* genotype frequency on the days from diagnosis to ART (n = 246).

	days from diagnosis to ART		
	88 days> (%)	88 days< (%)	p[a]
Genotype			
D/D	9 (3.7)	10 (4.1)	0.961
I/D	49 (19.9)	59 (24.0)	
I/I	57 (23.2)	62 (25.2)	

(Median days from diagnosis to ART = 88 days).
[a]Determined using the Fischer exact test.
The diagnosis date of 2 patients(each patient's genotype is I/I and I/D, respectively.) are unknown.
doi:10.1371/journal.pone.0092861.t004

1 replication, as shown in Figure 3. Similar to the HIV-1 results, overexpressed APOBEC3B potently suppresses HBV replication *in vitro* [36]. However, a study by Abe et al. on the frequency of the D/D genotype in HBV carriers demonstrated that the *APOBEC3B* gene deletion was not responsible for chronic HBV infection [37]. These data suggest that the high expression of APOBEC3B *in vitro* may produce exaggerated effects on both HIV-1 and HBV infection *in vitro*.

All the participants enrolled in this study were Japanese MSM, according to the information provided on anonymous questionnaires. Because approximately 80% of the HIV-1-positive patients in Japan are MSM [38], we investigated the effects of *APOBEC3B* deletion polymorphisms on this major mode of HIV-1 transmission rather than on the two other major modes (injection drug use and heterosexual intercourse). However, the effect of *APOBEC3B* genotype is less likely to be dependent on the mode of HIV-1 transmission because APOBEC3B mRNA expression in hematopoietic cells is lower and less tissue-specific than that of most of the other APOBEC3 family members [22,34,35].

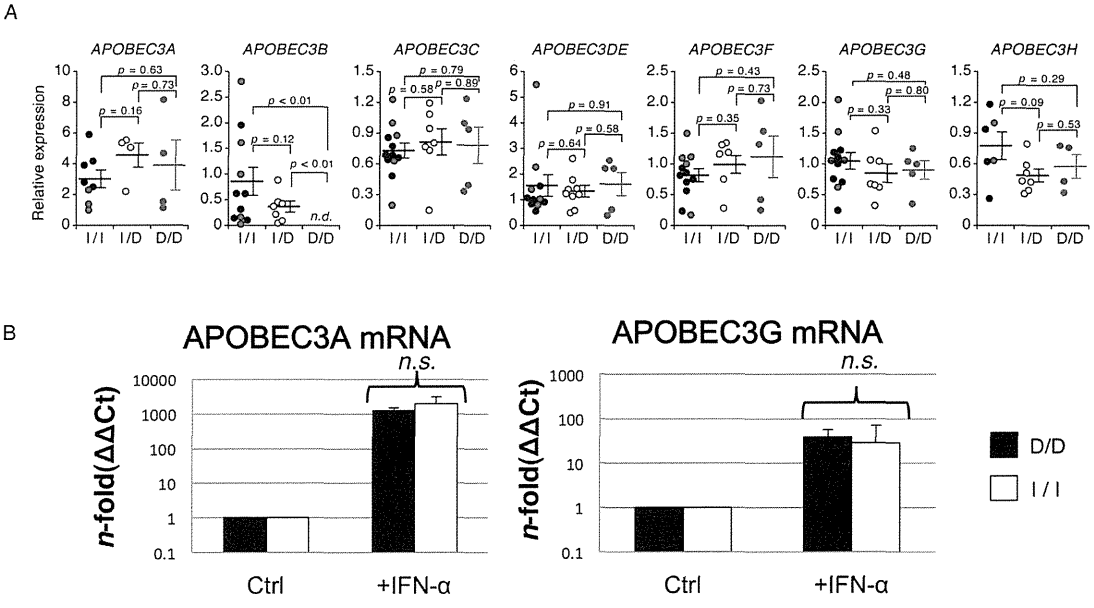

Figure 2. APOBEC3 mRNA expression levels depending on *APOBEC3B* genotype. (A) Comparison of mRNA expression levels of APOBEC3 in $CD4^+$ cells isolated from intact (I/I), hemizygous (I/D) and deletion (D/D) individuals of healthy donors. The relative mRNA expression levels of APOBEC3A (I/I, n = 8; I/D, n = 4; D/D, n = 4), APOBEC3B (I/I, n = 11; I/D, n = 7; D/D, n = 5), APOBEC3C (I/I, n = 12; I/D, n = 7; D/D, n = 5), APOBEC3DE (I/I, n = 11; I/D, n = 9; D/D, n = 5), APOBEC3F (I/I, n = 12; I/D, n = 7; D/D, n = 5), APOBEC3G (I/I, n = 12; I/D, n = 7; D/D, n = 5), and APOBEC3H (I/I, n = 6; I/D, n = 7; D/D, n = 4) were determined using quantitative RT-PCR and were normalized to GAPDH. The red (I/I) or gray (D/D) dots represent the expression levels of donors whose PBMCs were used for the *in vitro* kinetics of HIV-1 replication and infectivity in Figure. 3. The p values were calculated using Welch's *t*-test. The error bar represents the standard error of the mean (SEM). (B) APOBEC3A (A3A) and APOBEC3G (A3G) mRNA expression levels under basal conditions (Ctrl) and after stimulation with 100 U/ml (+IFN-α) of interferon (IFN)-α in $CD14^+$ MDMs isolated from healthy control subjects. The black and white bars indicate D/D (n = 3) and I/I (n = 4) individuals, respectively. The *p* values were calculated with the Mann-Whitney *U*-test. The error bars represent the standard deviation. *n.d.*, not detected. Ct, cycle threshold. *n.s.*, not significant ($p = 0.4$ for both cases).
doi:10.1371/journal.pone.0092861.g002

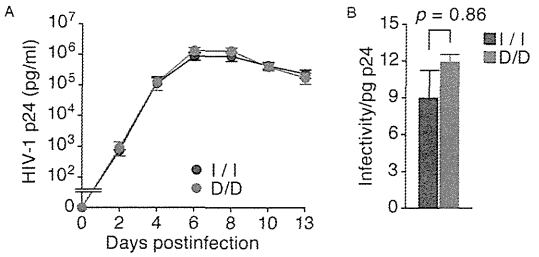

Figure 3. The kinetics and infectivity of HIV-1 depending on *APOBEC3B* genotype. (A) The kinetics of HIV-1 replication in PBMCs isolated from I/I (black dot) or D/D (gray dot) subjects (n = 5 each). (B) The infectivity values of virus-containing supernatants derived from I/I (black bar) and D/D (gray bar) PBMCs six days post-infection are provided relative to the values normalized with equal amounts of p24. The assay was performed using samples from three donors, and a representative result is shown. The p values were calculated using Welch's *t*-test. The error bars represent the SEM.
doi:10.1371/journal.pone.0092861.g003

In the D/D genotype, APOBEC3A mRNA expressed from the genome has a 3′-untranslated region corresponding to that of APOBEC3B. In addition, the genomic location of the APOBEC3G coding region is closer to the highly IFN-responsive transcriptional element of *APOBEC3A* in the D/D genome than to in the I/I. Therefore, we evaluated whether *APOBEC3B* gene deletion altered the IFN-stimulated gene induction of the other APOBEC3 family members. Our results suggest that the 29.5-kb genomic deletion of *APOBEC3B* does not significantly affect the expression profiles of the proximal *APOBEC3* family genes. Therefore, it is unlikely that the loss of the *APOBEC3B* gene in the D/D population leads to functional compensation via the mRNA expression modulation of the other APOBEC3 family members. Interestingly, Biasin et al. have demonstrated that increased levels of APOBEC3G mRNA in PBMCs, (primarily $CD14^+$ MDMs) following exposure to IFN-α correlated with HIV-1 susceptibility both *in vivo* and *in vitro* [13]. Our results showed that the induction magnitude of APOBEC3G mRNA upon the IFN-α stimulation was similar between the I/I and D/D genotypes (Figure 2B). This suggests that different HIV-1 susceptibility observed by Basin et al. is unlikely linked to the *APOBEC3B* intact/deletion genotypes.

Recent studies of tumors such as breast cancers [39–41] and lymphomas [42] have shown that increased expression of APOBEC3B *in vivo* was linked to the chronic induction of mutations and/or instability in genomic DNA. We did not observe any significant diagnosable HIV-associated cancers in our short-term cohort study. It may be necessary to continue our prospective studies for a longer period. In addition, because other studies have suggested that *APOBEC3B* gene deficiency is associated with higher susceptibility to two other ancient pathogens, human T-cell leukemia virus type 1 [43,44] and *Plasmodium falciparum* (the causative agent of malaria) [45], it would be beneficial to further investigate the correlations between *APOBEC3B* genotype and susceptibility to unknown pathogens.

Conclusions

Our analysis of a population-based matched cohort provided important evidence that the loss of the *APOBEC3B* gene is not associated with risk of HIV-1 infection and disease progression. In addition, the *in vitro* kinetics of HIV-1 replication and the infectivity of the virus in PBMCs were comparable between the D/D and I/I subjects. These results suggest that the APOBEC3B antiviral mechanism plays only a negligible role in eliminating HIV-1 *in vivo*. This finding may explain why HIV-1 has not evolved a Vif-based strategy to counteract APOBEC3B restriction. Further analyses to explore the role(s) of APOBEC3B in human are also required in other cohorts with diverse genetic backgrounds in Asia.

Supporting Information

Figure S1 Overexpression of two APOBEC3B variants and the antiviral effect of the variants *in vitro*. **(A)** A DNA fragment of the complete *APOBEC3B* open reading frame was amplified by RT-PCR from each RNA sample of healthy donors with APOBEC3B K62 (A3B K62) and E62 (A3B E62). Each of the fragment was replaced into the *APOBEC3G* gene position of the pcDNA A3G (Myc-His) WT (A3G WT) plasmid as previously described [8]. The primer sets for amplification of APOBEC3B cDNA were used as follows: the 1st PCR, 5′- gagcgggacagggacaagcg and 5′- aacccaggtctctgcctccc; the 2nd PCR, 5′- tcgagcggccgcatgaatccacagatcagaaatccg and 5′- cgatacaagcttgtttccctgattctggagaatggc. The resultant APOBEC3B expression plasmids, pcDNA APOBEC3B K62 and pcDNA APOBEC3B E62, contain a C-terminal MycHIS tag (consisting of Myc and hexa-histidine epitopes). The sequences of both the insert and the boundary regions for the APOBEC3B expression plasmids were verified by DNA sequencing. The expression or control (Vector) plasmids were transfected into human embryonic kidney cells (HEK 293T) by using FuGENE HD (Promega, Madison, USA). At 48 hr after transfection, cell lysates were prepared with Laemmli buffer containig 2.5% 2-Mercaptoethanol and analyzed by western blot. Protein bands were probed with anti-β-tubulin rabbit polyclonal antibody (1/2,500) (ab6046, Abcam, Cambridge, USA) or anti-His mAb (1/3,000) (D291-3, Medical & Biological Laboratories Co., Nagoya, Japan) as previously reported [8]. **(B)** The effect of two APOBEC3B variants on HIV-1 infectivity *in vitro* was analyzed. For virus production, 293T cells were cotransfected with 1 μg of pNL4-3 WT (HIV-1 WT) or pNL4-3*vif*(–) (HIV-1 *vif*(–)) plus 1 (black) or 0.1 (gray) μg of pcDNA APOBEC3B K62, pcDNA APOBEC3B E62, pcDNA 3.1 (–) (Vector), or pcDNA A3G (Myc-His) WT. Because it has been reported that the antiviral effect of APOBEC3B on HIV-1 *in vitro* can be observed when overexpressed in 293T cells but not T cell lines [20], we used 293T cells for the virus production. Virus infectivity was determined using TZM-bl cells [29]. Relative infectivity as relative light units (RLU) was calculated by normalizing for the amount of input CA, determined by p24 antigen ELISA (ZeptoMetrix, Buffalo, USA). Three independent experiments were performed. Results from one representative experiments are shown. A3G, APOBEC3G.
(TIF)

Figure S2 Quantitative hypermutation analysis of APOBEC3-prefered dinucleotide motifs in the proviral DNA isolated from PBMCs of HIV-1 (+) patients. **(A)** Genomic DNAs from patients' PBMC (n = 4, for each *APOBEC3B* genotype I/I, I/D, and D/D) were extracted using the QIAamp DNA Blood Mini Kit. The proviral DNA fragments were prepared by nested PCR using the PrimeSTAR GXL DNA Polymerase (Takara Bio). For the first PCR, a 2,877-bp DNA fragment of *pol* (RT-IN) region (nt 2,388–5,264 according to the numbering positions of HXB2 strain, K03455) and a 1,095-bp fragment of *vif* region (nt 4,899–5,993) were independently amplified with 300 nM of each primer set: *pol*, DRRT1L (5′-atgataggggggaattg-

gaggttt) and DRIN1R (5′-cctgtatgcagaccccaatatg); *vif*, DRVIF1F (5′-cgggtttattacagggacagcag) and DRVIF1R (5′-gctgtctccgcttcttcctgccat). For the nested PCR, a 2,735-bp (*pol*, nt 2,485–5,219) and an 859-bp (*vif*, nt 4,953–5,812) fragment were generated using primer sets, DRRT7L (5′-gacctacacctgtcaacataattgg)/DRRT7R (5′-cctagtgggatgtgtacttctgaactta) and DRVIF2F (5′-ctctggaaaggtgaaggggcagta)/DRVIF2R (5′-gaataatgcctattctgctatg), respectively. The resulting PCR products were purified with the QIAquick PCR Purification kit (Qiagen) and quantified with the Quant-iT dsDNA BR kit (Life Technologies). Paired-end DNA libraries were prepared using the Nextera DNA sample prep kit (Illumina, San Diego, USA) according to the manufacture's protocol. The DNA libraries were sequenced on a MiSeq (Illumina) using the MiSeq reagent kit v2 to produce 250 bp ×2 paired-end reads. The reads generated by deep sequencing were mapped onto the reference sequence of HXB2 strain by BWA 0.7.3a program (http://bio-bwa.sourceforge.net). Then, sequences of a 150-base pairs-long region were extracted and the sequences containing bases with quality scores under 30 were omitted by our *in house* program. **(B)** Among the extracted sequences, the hypermutation types and the numbers of the dinucletitide sequences, GG>AG (red) and GA>AA (blue), were analyzed. In order to detect hypermutations, the unique sequences with >5-fold coverage depth were used. The frequency (%) of hypermutaion is shown as mutation rates per dinucleotide (GG or GA) sequence with two color-coded scales below. The positions of the hypermutations in each patient sample are represented based on the nucleotide position of HXB2 strain. Since no sequences at the 3′-end part of *vif* (5470–5619) in sample ID #15, 47 and 73 were mapped onto HXB2 (panel A), the hypermutation frequency in the portion (5,485–5,619) is not shown. **(C)** The cumulative histograms represent number of hypermuated positions (y-axis) for GG>AG (red) or GA>AA (blue) at the degree of hypermutation (%) (x-axis). Bars were denoted for every 10% of the frequency degree.
(PDF)

Figure S3 Relative expression levels of APOBEC3B mRNA in three different *APOBEC3B* genotyped subjects of healthy donors or HIV-1-infected patients. Total RNA samples were isolated from PBMCs of three different genotyped subjects, intact (I/I); hemizygous (I/D); and deletion (D/D) individuals, of healthy donors (Uninfected), or HIV-1 (+) patients before (Naïve) or after (Treated) cART. Each genotype includes 3 samples for each status. Relative APOBEC3B mRNA expression levels were determined by using RT-qPCR using the Thermal Cycler Dice Real Time System (TP800) (Takara Bio, Shiga, Japan). The qPCR cycle at which amplification was detectable above a background threshold (threshold cycle, or Ct) was calculated and normalized to β-Actin. The relative expression levels are presented as the ΔΔCt (*n*-fold) of APOBEC3B mRNA to β-actin mRNA. cDNA sytheisis and qPCR was performed in duplicate for each sample, and the mean values and standard deviations for each genotype group (n = 3) are shown. The p values were calculated using Kruskal-Wallis test. The error bar represents the standard deviation. *n.d.*, not detected.
(TIF)

Table S1 Oligonucleotide primers used for real-time PCR of *APOBEC3* and control. A real-time PCR assay was performed for *APOBEC3* and control genes (Gene symbol) using each of forward primer (S) and reverse primer (AS) sets.
(DOC)

Table S2 APOBEC3B variations in the I/D and I/I genotyped healthy donors. APOBEC3B cDNAs from I/D and I/I-genotyped healthy donors (n = 5 each) were amplified by the nested RT-PCR and cloned into pUC118 plasmids. The *APOBEC3B* cDNA sequences were determined by DNA sequencing. The individual APOBEC3B variants analyzed are shown. A3B, APOBEC3B.
(DOC)

Acknowledgments

The authors thank all of the patients and volunteers who agreed to participate in this study. We also thank the NLGR organization for cooperating in the recruitment of the MSM volunteers in Nagoya. The TZM-bl cells were provided by J. C. Kappes and X. Wu through the AIDS Research and Reference Reagent Program, Division of AIDS, NIAID, National Institutes of Health, NIH Reagent Program.

Author Contributions

Conceived and designed the experiments: MI TI NK SI YK ATK MU YY WS YI TN. Performed the experiments: MI TI KM TM KS YI. Analyzed the data: MI TI DW JI KS HO YK ATK YY WS YI. Contributed reagents/materials/analysis tools: MI DW JI SI MU YY TS. Wrote the paper: MI TI YK ATK WS YI TN.

References

1. Albin JS, Harris RS (2010) Interactions of host APOBEC3 restriction factors with HIV-1 in vivo: implications for therapeutics. Expert Rev Mol Med 12: e4.
2. Goila-Gaur R, Strebel K (2008) HIV-1 Vif, APOBEC, and intrinsic immunity. Retrovirology 5: 51.
3. Sheehy AM, Gaddis NC, Choi JD, Malim MH (2002) Isolation of a human gene that inhibits HIV-1 infection and is suppressed by the viral Vif protein. Nature 418: 646–650.
4. Bishop KN, Verma M, Kim EY, Wolinsky SM, Malim MH (2008) APOBEC3G inhibits elongation of HIV-1 reverse transcripts. PLoS Pathog 4: e1000231.
5. Iwatani Y, Chan DS, Wang F, Maynard KS, Sugiura W, et al. (2007) Deaminase-independent inhibition of HIV-1 reverse transcription by APOBEC3G. Nucleic Acids Res 35: 7096–7108.
6. LaRue RS, Andrésdóttir V, Blanchard Y, Conticello SG, Derse D, et al. (2009) Guidelines for naming nonprimate APOBEC3 genes and proteins. J Virol 83: 494–497.
7. Yu X, Yu Y, Liu B, Luo K, Kong W, et al. (2003) Induction of APOBEC3G ubiquitination and degradation by an HIV-1 Vif-Cul5-SCF complex. Science 302: 1056–1060.
8. Kitamura S, Ode H, Nakashima M, Imahashi M, Naganawa Y, et al. (2012) The APOBEC3C crystal structure and the interface for HIV-1 Vif binding. Nat Struct Mol Biol 19: 1005–1010.
9. Li MM, Wu LI, Emerman M (2010) The range of human APOBEC3H sensitivity to lentiviral Vif proteins. J Virol 84: 88–95.
10. Russell RA, Smith J, Barr R, Bhattacharyya D, Pathak VK (2009) Distinct domains within APOBEC3G and APOBEC3F interact with separate regions of human immunodeficiency virus type 1 Vif. J Virol 83: 1992–2003.
11. Smith JL, Pathak VK (2010) Identification of specific determinants of human APOBEC3F, APOBEC3C, and APOBEC3DE and African green monkey APOBEC3F that interact with HIV-1 Vif. J Virol 84: 12599–12608.
12. Zhen A, Wang T, Zhao K, Xiong Y, Yu XF (2010) A single amino acid difference in human APOBEC3H variants determines HIV-1 Vif sensitivity. J Virol 84: 1902–1911.
13. Biasin M, Piacentini L, Lo Caputo S, Kanari Y, Magri G, et al. (2007) Apolipoprotein B mRNA-editing enzyme, catalytic polypeptide-like 3G: a possible role in the resistance to HIV of HIV-exposed seronegative individuals. J Infect Dis 195: 960–964.
14. Chaipan C, Smith JL, Hu WS, Pathak VK (2013) APOBEC3G restricts HIV-1 to a greater extent than APOBEC3F and APOBEC3DE in human primary CD4+ T cells and macrophages. J Virol 87: 444–453.
15. Do H, Vasilescu A, Diop G, Hirtzig T, Heath SC, et al. (2005) Exhaustive genotyping of the CEM15 (APOBEC3G) gene and absence of association with AIDS progression in a French cohort. J Infect Dis 191: 159–163.
16. Kourteva Y, De Pasquale M, Allos T, McMunn C, D'Aquila RT (2012) APOBEC3G expression and hypermutation are inversely associated with human immunodeficiency virus type 1 (HIV-1) burden in vivo. Virology 430: 1–9.

17. Mulder LC, Ooms M, Majdak S, Smedresman J, Linscheid C, et al. (2010) Moderate influence of human APOBEC3F on HIV-1 replication in primary lymphocytes. J Virol 84: 9613–9617.
18. Ulenga NK, Sarr AD, Thakore-Meloni S, Sankale JL, Eisen G, et al. (2008) Relationship between human immunodeficiency type 1 infection and expression of human APOBEC3G and APOBEC3F. J Infect Dis 198: 486–492.
19. Vetter ML, Johnson ME, Antons AK, Unutmaz D, D'Aquila RT (2009) Differences in APOBEC3G expression in CD4+ T helper lymphocyte subtypes modulate HIV-1 infectivity. PLoS Pathog 5: e1000292.
20. Hultquist JF, Lengyel JA, Refsland EW, LaRue RS, Lackey L, et al. (2011) Human and rhesus APOBEC3D, APOBEC3F, APOBEC3G, and APOBEC3H demonstrate a conserved capacity to restrict Vif-deficient HIV-1. J Virol 85: 11220–11234.
21. Pak V, Heidecker G, Pathak VK, Derse D (2011) The role of amino-terminal sequences in cellular localization and antiviral activity of APOBEC3B. J Virol 85: 8538–8547.
22. Yu Q, Chen D, Konig R, Mariani R, Unutmaz D, et al. (2004) APOBEC3B and APOBEC3C are potent inhibitors of simian immunodeficiency virus replication. J Biol Chem 279: 53379–53386.
23. Bishop KN, Holmes RK, Sheehy AM, Davidson NO, Cho SJ, et al. (2004) Cytidine deamination of retroviral DNA by diverse APOBEC proteins. Curr Biol 14: 1392–1396.
24. Doehle BP, Schafer A, Cullen BR (2005) Human APOBEC3B is a potent inhibitor of HIV-1 infectivity and is resistant to HIV-1 Vif. Virology 339: 281–288.
25. Kidd JM, Newman TL, Tuzun E, Kaul R, Eichler EE (2007) Population stratification of a common APOBEC gene deletion polymorphism. PLoS Genet 3: e63.
26. An P, Johnson R, Phair J, Kirk GD, Yu XF, et al. (2009) APOBEC3B deletion and risk of HIV-1 acquisition. J Infect Dis 200: 1054–1058.
27. Itaya S, Nakajima T, Kaur G, Terunuma H, Ohtani H, et al. (2010) No evidence of an association between the APOBEC3B deletion polymorphism and susceptibility to HIV infection and AIDS in Japanese and Indian populations. J Infect Dis 202: 815–816; author reply 816–817.
28. Bogerd HP, Cullen BR (2008) Single-stranded RNA facilitates nucleocapsid: APOBEC3G complex formation. RNA 14: 1228–1236.
29. Iwatani Y, Takeuchi H, Strebel K, Levin JG (2006) Biochemical activities of highly purified, catalytically active human APOBEC3G: correlation with antiviral effect. J Virol 80: 5992–6002.
30. Svarovskaia ES, Xu H, Mbisa JL, Barr R, Gorelick RJ, et al. (2004) Human apolipoprotein B mRNA-editing enzyme-catalytic polypeptide-like 3G (APOBEC3G) is incorporated into HIV-1 virions through interactions with viral and nonviral RNAs. J Biol Chem 279: 35822–35828.
31. Burnett A, Spearman P (2007) APOBEC3G multimers are recruited to the plasma membrane for packaging into human immunodeficiency virus type 1 virus-like particles in an RNA-dependent process requiring the NC basic linker. J Virol 81: 5000–5013.
32. Wichroski MJ, Robb GB, Rana TM (2006) Human retroviral host restriction factors APOBEC3G and APOBEC3F localize to mRNA processing bodies. PLoS Pathog 2: e41.
33. Stenglein MD, Harris RS (2006) APOBEC3B and APOBEC3F inhibit L1 retrotransposition by a DNA deamination-independent mechanism. J Biol Chem 281: 16837–16841.
34. Koning FA, Newman EN, Kim EY, Kunstman KJ, Wolinsky SM, et al. (2009) Defining APOBEC3 expression patterns in human tissues and hematopoietic cell subsets. J Virol 83: 9474–9485.
35. Refsland EW, Stenglein MD, Shindo K, Albin JS, Brown WL, et al. (2010) Quantitative profiling of the full APOBEC3 mRNA repertoire in lymphocytes and tissues: implications for HIV-1 restriction. Nucleic Acids Res 38: 4274–4284.
36. Bonvin M, Greeve J (2007) Effects of point mutations in the cytidine deaminase domains of APOBEC3B on replication and hypermutation of hepatitis B virus in vitro. J Gen Virol 88: 3270–3274.
37. Abe H, Ochi H, Maekawa T, Hatakeyama T, Tsuge M, et al. (2009) Effects of structural variations of APOBEC3A and APOBEC3B genes in chronic hepatitis B virus infection. Hepatol Res 39: 1159–1168.
38. Hattori J, Shiino T, Gatanaga H, Yoshida S, Watanabe D, et al. (2010) Trends in transmitted drug-resistant HIV-1 and demographic characteristics of newly diagnosed patients: nationwide surveillance from 2003 to 2008 in Japan. Antiviral Res 88: 72–79.
39. Burns MB, Lackey L, Carpenter MA, Rathore A, Land AM, et al. (2013) APOBEC3B is an enzymatic source of mutation in breast cancer. Nature 494: 366–370.
40. Burns MB, Temiz NA, Harris RS (2013) Evidence for APOBEC3B mutagenesis in multiple human cancers. Nat Genet 45: 977–983.
41. Xuan D, Li G, Cai Q, Deming-Halverson S, Shrubsole MJ, et al. (2013) APOBEC3 deletion polymorphism is associated with breast cancer risk among women of European ancestry. Carcinogenesis.
42. Shinohara M, Io K, Shindo K, Matsui M, Sakamoto T, et al. (2012) APOBEC3B can impair genomic stability by inducing base substitutions in genomic DNA in human cells. Sci Rep 2: 806.
43. Mahieux R, Suspene R, Delebecque F, Henry M, Schwartz O, et al. (2005) Extensive editing of a small fraction of human T-cell leukemia virus type 1 genomes by four APOBEC3 cytidine deaminases. J Gen Virol 86: 2389–2394.
44. Ooms M, Krikoni A, Kress AK, Simon V, Munk C (2012) APOBEC3A, APOBEC3B, and APOBEC3H haplotype 2 restrict human T-lymphotropic virus type 1. J Virol 86: 6097–6108.
45. Jha P, Sinha S, Kanchan K, Qidwai T, Narang A, et al. (2012) Deletion of the APOBEC3B gene strongly impacts susceptibility to falciparum malaria. Infect Genet Evol 12: 142–148.

Organic & Biomolecular Chemistry

PAPER

View Article Online
View Journal | View Issue

Cite this: Org. Biomol. Chem., 2014, 12, 5006

Design and synthesis of lipid-coupled inositol 1,2,3,4,5,6-hexakisphosphate derivatives exhibiting high-affinity binding for the HIV-1 MA domain†

Hiroshi Tateishi,‡[a] Kensaku Anraku,‡[b] Ryoko Koga,[a] Yoshinari Okamoto,[a] Mikako Fujita[c] and Masami Otsuka*[a]

Received 15th February 2014,
Accepted 13th May 2014

DOI: 10.1039/c4ob00350k

www.rsc.org/obc

The precursor of Gag protein ($Pr55^{Gag}$) of human immunodeficiency virus, the principal structural component required for virus assembly, is known to bind D-*myo*-phosphatidylinositol 4,5-bisphosphate (PIP_2). The N-terminus of $Pr55^{Gag}$, the MA domain, plays a critical role in the binding of $Pr55^{Gag}$ to the plasma membrane. Herein, we designed and synthesized *myo*-phosphatidylinositol 2,3,4,5,6-pentakisphosphate (PIP_5) derivatives comprising highly phosphorylated inositol and variously modified diacylglycerol to examine the MA-binding properties. The inositol moiety was synthesized starting with *myo*-inositol and assembled with a hydrophobic glycerol moiety through a phosphate linkage. The K_d value for MA-binding of the PIP_5 derivative **2** (K_d = 0.25 μM) was the lowest (*i.e.*, highest affinity) of all derivatives, *i.e.*, 70-fold lower than the K_d for the PIP_2 derivative **1** (K_d = 16.9 μM) and 100-fold lower than the K_d for IP_6 (K_d = 25.7 μM), suggesting the possibility that the PIP_5 derivative blocks $Pr55^{Gag}$ membrane binding by competing with PIP_2 in MA-binding.

1. Introduction

The development of anti-human immunodeficiency virus type 1 (HIV-1) drugs has achieved marked success in the past two decades as envisaged by reverse transcriptase inhibitors, protease inhibitors, entry inhibitors, and integrase inhibitors. However, because the use of these drugs has encountered limitations because of the emergence of resistant viral variants, the development of new drugs based on novel mechanisms has become urgent. This study focused on the membrane targeting of the HIV-1 precursor of Gag protein ($Pr55^{Gag}$) at the stage of virus assembly, exploiting the possibility to block the virus assembly by small molecules that compete at the membrane binding of $Pr55^{Gag}$.

HIV-1 genome-encoded $Pr55^{Gag}$ protein is the principal structural component required for virus assembly.[1,2] Following ribosomal synthesis, $Pr55^{Gag}$ is directed to the plasma membrane, where it is assembled with other components to form immature budding virions. The N-terminus of $Pr55^{Gag}$, the MA domain, plays a critical role in the binding of $Pr55^{Gag}$ to the plasma membrane.[3] Recent studies have shown that D-*myo*-phosphatidylinositol 4,5-bisphosphate (PIP_2) is the binding target of the basic patch of the MA domain.[4–6]

We previously developed a highly sensitive *in vitro* assay to determine the binding affinity of $Pr55^{Gag}$/MA for phosphoinositide derivatives by employing a surface plasmon resonance (SPR) sensor in which a synthetic biotinylated inositol phosphate was immobilized.[7–9] The SPR experiments comparing the $Pr55^{Gag}$/MA affinity of IP_3 and PIP_2 suggested that both the divalent phosphate groups and the acyl chains of PIP_2 are essential for tight binding to $Pr55^{Gag}$/MA.

Because the PIP_2-binding region of the MA domain contains many basic residues that interact with acidic phosphate groups of the inositol,[2,10,11] the MA-binding affinity of phosphatidylinositol derivatives would be increased by increasing the number of phosphate groups. This, together with several previously published studies,[2,10,11] would provide the basis for the molecular design of novel competitors that would block the PIP_2-$Pr55^{Gag}$ binding.

Herein, we performed an SPR analysis of the MA domain binding of highly phosphorylated inositol phosphates, *myo*-inositol 1,2,3,4,5,6-hexakisphosphate (IP_6), D-*myo*-inositol 1,4,5-trisphosphate (IP_3), and a synthetic PIP_2 derivative

[a]Department of Bioorganic Medicinal Chemistry, Faculty of Life Sciences, Kumamoto University, 5-1 Oe-honmachi, Chuo-ku, Kumamoto 862-0973, Japan. E-mail: motsuka@gpo.kumamoto-u.ac.jp; Fax: +81-96-371-4620; Tel: +81-96-371-4620
[b]Department of Medical Technology, Kumamoto Health Science University, 325 Izumi-machi, Kita-ku, Kumamoto 861-5598, Japan
[c]Research Institute for Drug Discovery, School of Pharmacy, Kumamoto University, 5-1 Oe-honmachi, Chuo-ku, Kumamoto 862-0973, Japan

†Electronic supplementary information (ESI) available. See DOI: 10.1039/c4ob00350k

‡These authors contributed equally to this work.

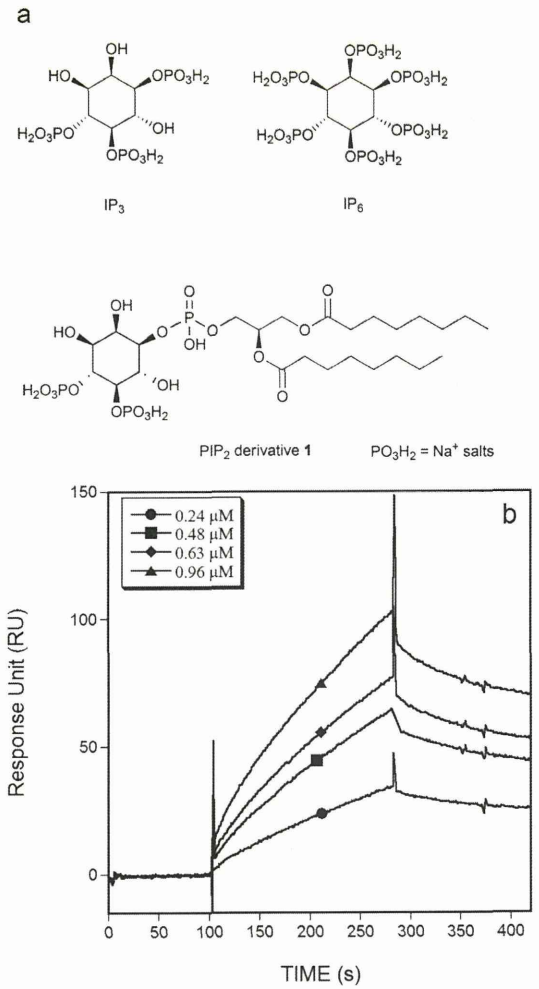

Fig. 1 Structures of IP_3, IP_6, and the PIP_2 derivative **1** (a). Binding activity of 0.24, 0.48, 0.64 and 0.96 μM MA proteins to biotinylated IP_4. Each protein was injected over a biotinylated IP_4-immobilized sensor chip at a flow rate of 20 μl min^{-1} for 180 s (b).

having non-natural C8 acyl chains **1** (Fig. 1a) and found that IP_6 bound MA strongly, demonstrating the significance of the number of phosphate groups. Further, we designed and synthesized lipid-coupled IP_6 derivatives, namely *myo*-phosphatidylinositol 2,3,4,5,6-pentakisphosphate (PIP_5) derivatives, expecting that their MA binding would be stronger than PIP_2, leading to the blockade of the $Pr55^{Gag}$ membrane target.

2. Results and discussion

2.1. SPR analysis of MA-interaction of IP_3, IP_6, and PIP_2

To compare the relative MA-binding affinity of IP_6, IP_3, and the PIP_2 derivative **1** (Fig. 1a), we performed an SPR assay that we had previously constructed.[7] An expression vector for MA having a FLAG tag at the C-terminus was used. Proteins were purified from transfected 293 T cells using anti-FLAG agarose beads employing the FLAG tag affinity method. Purified proteins were quantified by SDS-PAGE analysis, and their concentration was estimated by comparing the band intensity with that of the protein marker. After purification, the solution in which each protein was dissolved was exchanged with flow buffer in the SPR system through dialysis. Flow buffer was supplemented with 0.5 mg mL^{-1} BSA to inhibit non-selective binding to the biotin-modified control surface, followed by 2% (v/v) glycerol to prevent protein destabilization.[12] Contrary to the previous SPR analysis,[7] 5% dimethylsulfoxide was also supplemented with analysis buffer to dissolve complexes in this experiment (ESI 2†). Association was followed for 3 min and dissociation was measured at a flow rate of 20 μl min^{-1} at 25 °C, after which the surfaces were regenerated by injecting dilute NaOH solution. As shown in Fig. 1b, the injection of 0.24, 0.48, 0.64, and 0.96 μM MA into immobilized D-*myo*-inositol 1,3,4,5-tetrakisphosphate (IP_4) showed a concentration-dependent response unit (RU).

The dissociation constants (K_d) of MA–IP_3, MA–IP_6, and MA–**1** complexes were calculated *via* a competition assay. Solutions containing varying concentrations of each competitor were preincubated with MA and passed over the immobilized IP_4 surface. The competition curves were obtained by setting the concentration of competitors upon the horizontal axis and the response of free MA, determined based on the concentration of MA bound to immobilized-IP_4, upon the vertical axis. The RU curves for competition between MA and the various competitors are shown in Fig. 2a,c and e; the corresponding K_d values are shown in Fig. 2b,d and f. The K_d value for MA in competition with IP_3 was 272 μM (Fig. 2b), indicating that IP_3 binds MA weakly. It was noteworthy that IP_6 showed K_d (25.7 μM) (Fig. 2d) comparable to that of **1** (16.9 μM) (Fig. 2f), although IP_6 does not possess the diacylglycerol moiety. These findings suggested that MA-affinity would be further increased by introducing a diacylglycerol into IP_6.

2.2. Design and synthetic strategy of PIP_5 derivatives

We designed PIP_5 derivatives having a modified glycerol moiety (Fig. 3). To compare the influence of the aliphatic chain structure of the glycerol group, both acyl (compound **2**) and alkyl ether (compound **4**) derivatives were designed. To confirm that the 2′-acyl chain participates in PIP_2-MA binding and the 1′-acyl does not,[5] 1′-*O*-methyl-2′-acyl/alkyl derivatives (compounds **3** and **4**) were designed. Our synthetic strategy for the PIP_5 derivatives (Fig. 3) was to differentiate the six hydroxyl groups of *myo*-inositol through the diacetal intermediate,[13] and the suitably protected intermediate was coupled with an acyl/alkyl-glycerol moiety by a bifunctional phosphorylating agent.[14] A 1,5-dihydro-2,4,3-benzodioxaphosphepin-3-yl group was employed for the synthesis of the acyl derivatives (*i.e.*, **12**), whereas the 2-cyanoethyl group was used for the phosphorylating agent of the alkyl ether derivatives (*i.e.*, **12**).

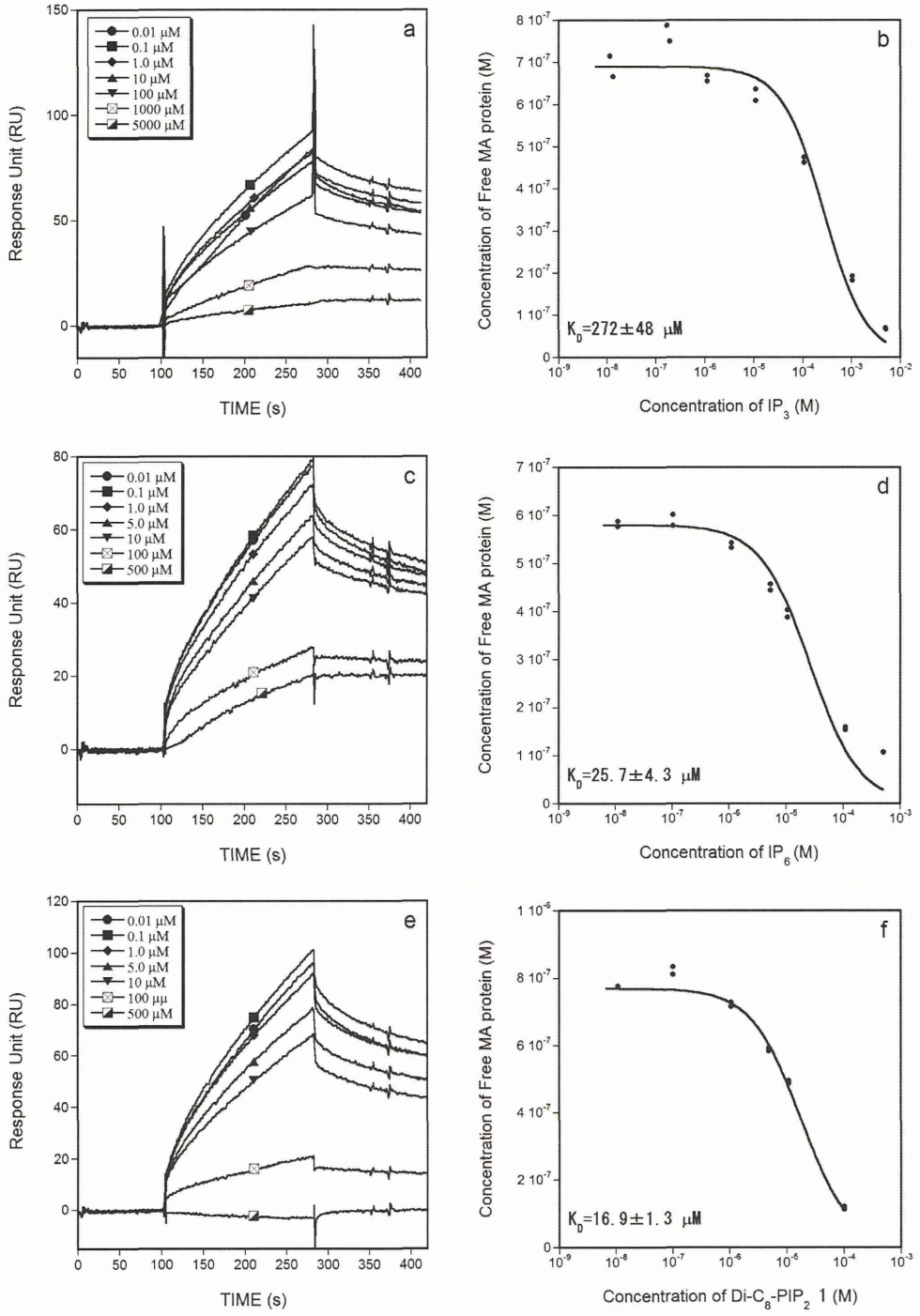

Fig. 2 Competition assay and calculation of the equilibrium dissociation constants (K_d) for MA-competitor complexes. The equilibrium mixtures of MA and competitors IP_3 (a), IP_6 (c), and the PIP_2 derivative **1** (e) were injected over the biotinylated IP_4-immobilized sensor chip at a flow rate of 20 μl min^{-1} for 180 s. The average response unit (RU) for the increasing concentration of each competitor was measured at 160–170 s, and each RU datum was converted to a concentration of uncompetitive MA protein used for the construction of competition curves between uncompetitive MA and IP_3 (b), IP_6 (d), and the PIP_2 derivative **1** (f). Calculated K_d values are shown. Each experiment was performed in duplicate.

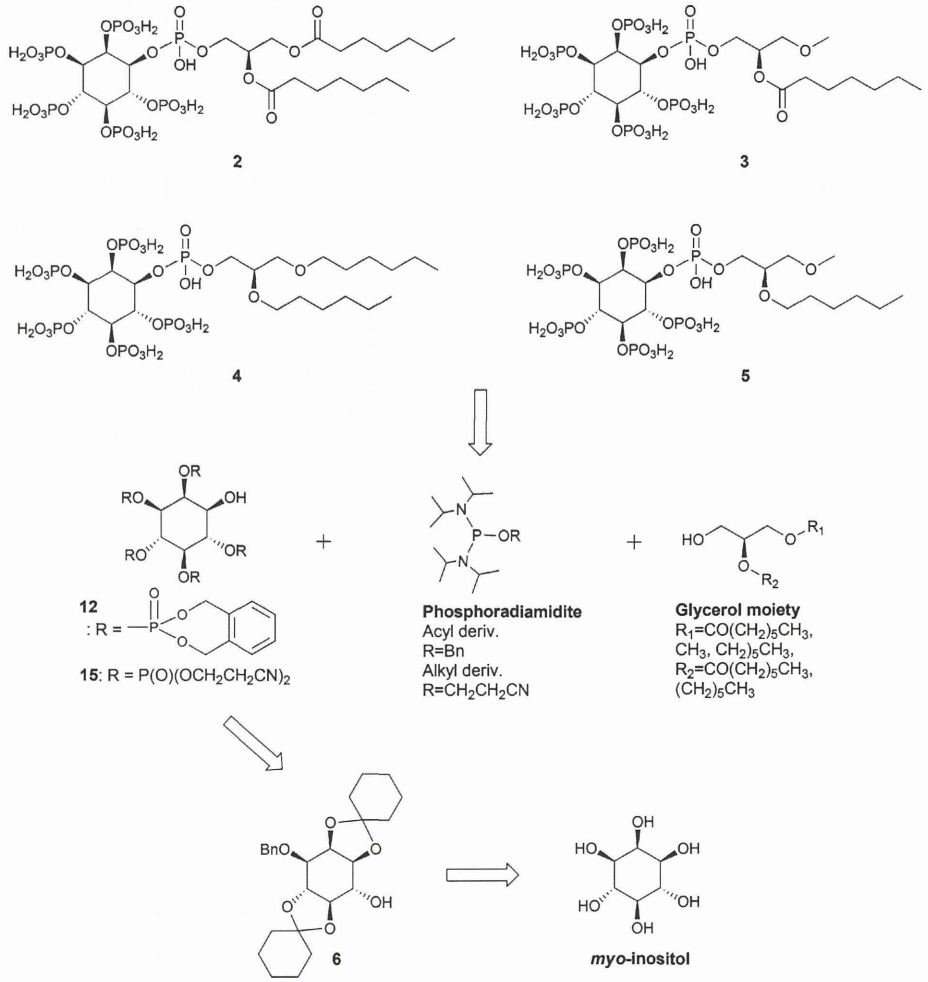

Fig. 3 Design and synthetic strategy of PIP_5 derivatives.

2.3. Syntheses of the IP_6 moiety

The syntheses of the IP_6 moiety for acyl derivatives were performed as shown in Scheme 1. The starting material DL-3-*O*-benzyl-1,2:4,5-di-*O*-cyclohexylidene-*myo*-inositol **6** was prepared according to the method of Billington *et al.*[13] Benzylation of the alcohol **6** provided **7**, which was further treated with *p*-toluenesulfonic acid and H_2O to give deacetalized **8** in 76% yield (for 2 steps). The *cis*-1,2-diol of **8** was regioselectively *p*-methoxybenzylated by means of the dibutyltin oxide procedure.[15,16] Thus, the tin complex of the 1,2-diol was reacted with *p*-methoxybenzyl chloride in the presence of cesium fluoride to give regioselectively protected **9** in 89% yield. The selective deprotection of the benzyl group of **9** by the method of Oikawa *et al.*[17] gave **10** in 45% yield. The 2,3,4,5,6-pentahydroxy compound **10** was converted to the corresponding pentakisphosphonate **11** by treatment with (1,5-dihydro-2,4,3-benzodioxaphosphepin-3-yl)diethylamine[18] and 1*H*-tetrazole and subsequent oxidation with MCPBA in 75% yield. Oxidative cleavage of the *p*-methoxybenzyl group with CAN[19] gave the desired IP_6 fragment **12**, accompanying a phosphate migration product **13** in which the *O*-xylyl protected phosphate group at the 2-phosphate group migrated to the 1-phosphate allocating a stable conformation of *myo*-inositols.[18] Because compounds **12** and **13** could not be separated, the mixture was used for the next coupling reaction without separation.

The synthesis of the IP_6 moiety for alkyl ether derivatives was performed as shown in Scheme 2. The 2,3,4,5,6-pentahydroxy compound **10** was converted to the corresponding pentakisphosphonate **14** by treatment with bis(2-cyanoethyl)-*N*,*N*-diisopropylphosphoramidite[20] and 1*H*-tetrazole and subsequent oxidation with MCPBA in 73% yield. Oxidative cleavage of the *p*-methoxybenzyl group with CAN[19] gave the IP_6 fragment **15** in 68% yield.

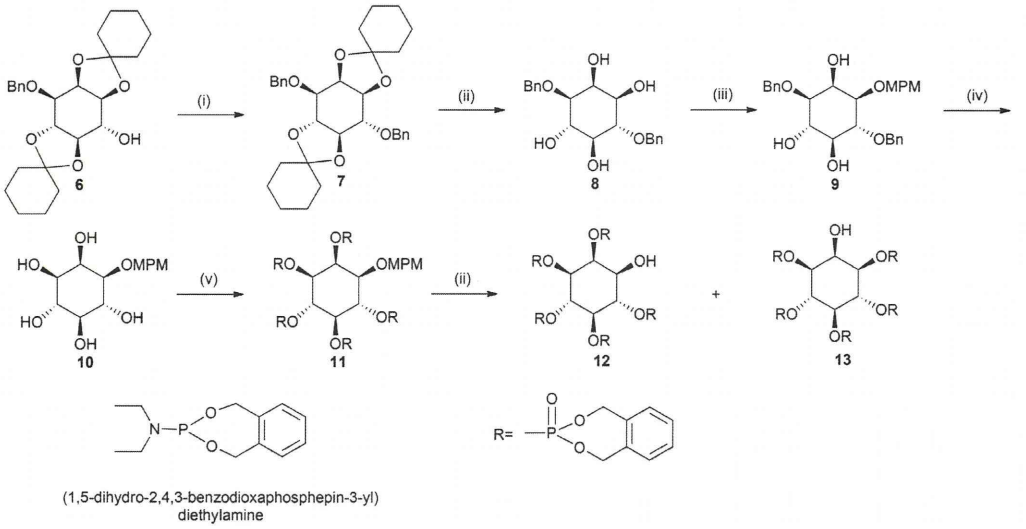

Scheme 1 *Reagents and conditions*: (i) benzyl bromide, NaH, DMF, rt, overnight, 94%; (ii) TsOH, THF–H_2O, reflux, 5 h, 81%; (iii) (a) Bu_2SnO, toluene, reflux, 3 h; (b) CsF, MPM-Cl, DMF, –40 °C then rt, 48 h, 89%; (iv) H_2/W-2 RANEY®-Ni, MeOH, 50 °C, 3 h, 45%; (v) (a) (1,5-dihydro-2,4,3-benzodioxaphosphepin-3-yl)diethylamine, 1*H*-tetrazole, CH_2Cl_2, rt, overnight; (b) MCPBA, CH_2Cl_2, –40 °C then rt, 1 h, 75%; (x) CAN, CH_3CN–H_2O, rt, 1 h.

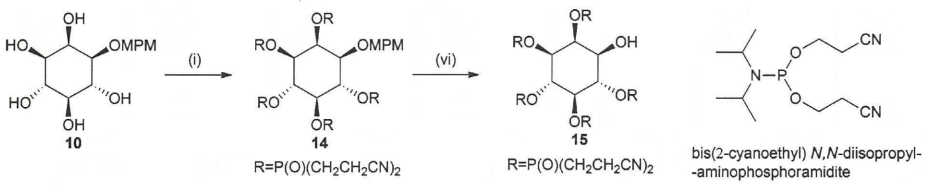

Scheme 2 *Reagents and conditions*: (i) (a) bis(2-cyanoethyl)-*N*,*N*-diisopropylaminophosphoramidite, 1*H*-tetrazole, CH_2Cl_2, rt, 1.5 h; (b) MCPBA, CH_2Cl_2, –78 °C then rt, 5 min, 73%; (ii) CAN, CH_3CN–H_2O, rt, 1.5 h, 68%.

2.4. Syntheses of di/mono-acylglycerol and di/mono-alkylglycerol moieties

The syntheses of diacylglycerol and dialkylglycerol moieties were performed as shown in Scheme 3. The commercially available starting material (*R*)-3-benzyloxy-1,2-propanediol **16** was reacted with heptanoyl chloride under basic conditions to give compound **17** in 86% yield. The deprotection of the benzyl group of **17** gave **18** in 96% yield. Compound **20** was obtained by dialkylation of **16** followed by the benzyl deprotection in 59% yield (for 2 steps).

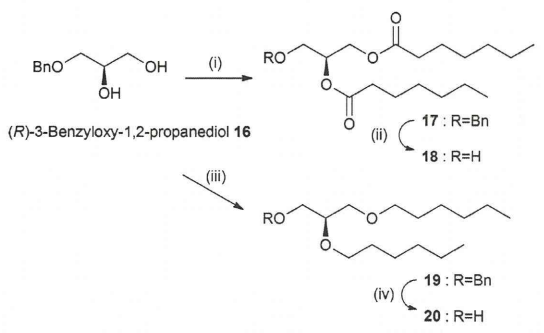

Scheme 3 *Reagents and conditions*: (i) heptanoyl chloride, DMAP, pyridine, CH_2Cl_2, overnight, 86%; (ii) H_2/Pd–C, CH_2Cl_2, overnight, 96%; (iii) hexyl bromide, NaH, DMF, rt, overnight, 70%; (iv) H_2/Pd–C, CH_2Cl_2, 24 h, 84%.

The syntheses of the monoacylglycerol and monoalkylglycerol moieties were performed as shown in Scheme 4. Compound **16** was regioselectively methylated by means of the dibutyltin oxide procedure. The tin complex of the 1,2-diol was reacted with methyl iodide in the presence of cesium fluoride to give **21** in 71% yield, accompanying a small amount of 2-*O*-methyl product. Acylation of the 2-hydroxyl of **21** with heptanoyl chloride gave **22** in 93% yield. The deprotection of the benzyl group of **22** gave **23** in 93% yield. Alkylation of the 2-hydroxyl of **21** with hexyl chloride gave **24** in 92% yield. Finally, compound **24** was treated with H_2/10% palladium carbon to afford the debenzylated product **25** in 89% yield.

2.5. Coupling of IP_6 and glycerol fragments

The coupling of acylated glycerol moieties and IP_6 fragments was performed as shown in Scheme 5. The glycerol moiety **18**

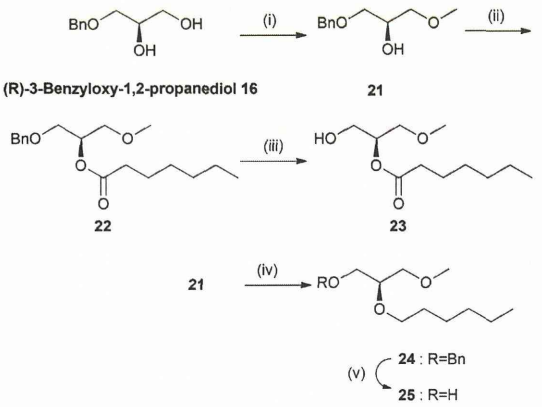

Scheme 4 *Reagents and conditions*: (i) (a) Bu_2SnO, toluene, reflux, 3 h; (b) CsF, methyl iodide, DMF, −40 °C then rt, 2 days, 71%; (ii) heptanoyl chloride, DMAP, pyridine, CH_2Cl_2, overnight, 93%; (iii) H_2/Pd–C, CH_2Cl_2, overnight, 93%; (iv) hexyl-Br, NaH, DMF, rt, overnight, 92%; (v) H_2/Pd–C, CH_2Cl_2, 24 h, 89%.

was reacted with benzyl-*N*,*N*,*N*′,*N*′-tetraisopropylphosphoramidite[14] and 1*H*-tetrazole and subsequently condensed with the IP_6 fragment mixture of **12** and **13**. Oxidation with *tert*-BuOOH gave diheptanoyl glyceryl IP_6 **26** and **27** in 22% and 45% yield, respectively. Finally, the protecting groups were removed by hydrogenolysis with palladium carbon to give diheptanoyl glyceryl PIP_5 derivatives. These PIP_5 derivatives were purified by cation-exchange chromatography to give **2** and its isomer **2**′ as triethylammonium salts in 34% and 35% yield, respectively.

The monoacylglycerol derivatives, **3** and its isomer **3**′ as triethylammonium salts, were synthesized by the same procedure.

The coupling reaction of the IP_6 fragment and the alkylated glycerol moieties was performed as shown in Scheme 6. The glycerol moiety **20** or **25** was reacted with the bifunctional phosphorylating agent (2-cyanoethyl)-*N*,*N*,*N*′,*N*′-tetraisopropylphosphoramidite[14] and 1*H*-tetrazole to yield a rather labile phosphoramidite. This compound was condensed with the IP_6 fragment **20** or **25** without further purification. Oxidation of the condensed product with *tert*-BuOOH gave 1,2-*O*-dihexylglyceryl or 1-*O*-methyl-2-*O*-hexyl IP_6 **30** or **31** in 41% and 63% yield, respectively. Finally, protecting groups were removed by reaction with NH_3 to give water-soluble PIP_5 derivatives that were purified by reverse phase chromatography followed by cation-exchange chromatography to give **4** and **5** as triethylammonium salts in 64% and 31% yield, respectively.

2.6. SPR analysis of MA complexes of PIP_5 derivatives

K_d values of the MA complex of PIP_5 derivatives were calculated by the competition assay as described above. The RU curves for competition between MA and the various competitors are shown in Fig. 4a,c,e,g,i and k; the corresponding K_d values are shown in Fig. 4b,d,f,h,j and l. As illustrated in Fig. 5, which shows the K_d of the MA complex of IP_3, IP_6, the PIP_2 derivative **1**, and PIP_5 derivatives with structure, the K_d values for MA in competition with **2** (K_d = 0.25 μM) (Fig. 4b) were the lowest (*i.e.*, highest affinity) of all PIP_5 derivatives, which was 70-fold lower than the K_d for **1** (16.9 μM) and 100-fold lower than the K_d for IP_6 (25.7 μM). Therefore, the K_d value of the **2**-MA complex showed that PIP_5 derivatives having both IP_6 and

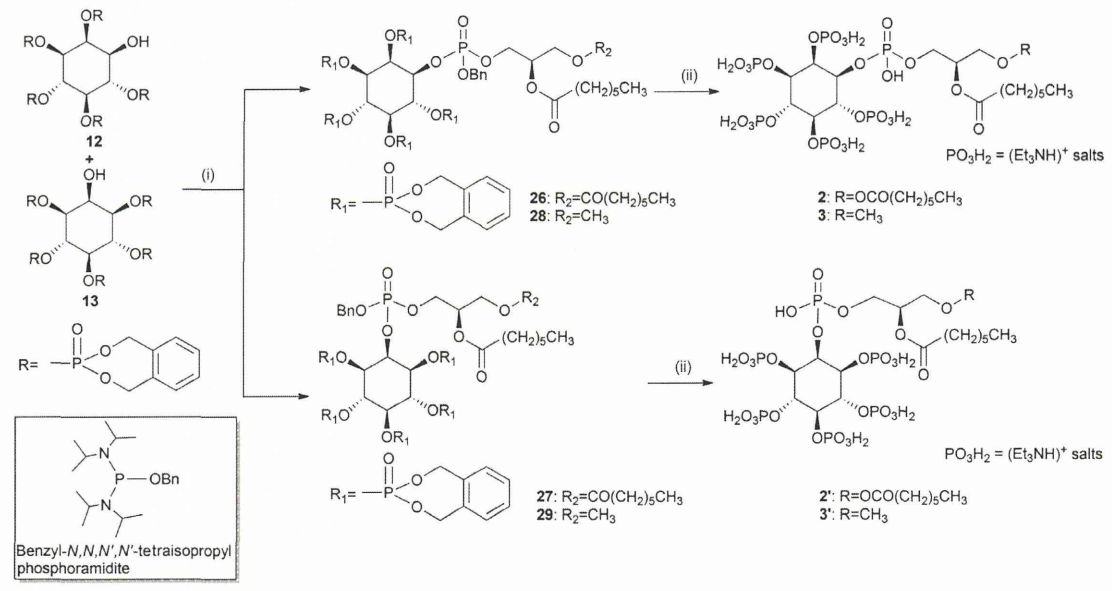

Scheme 5 *Reagents and conditions*: (i) (a) benzyl-*N*,*N*,*N*′,*N*′-tetraisopropylphosphoramidite, 1*H*-tetrazole, CH_2Cl_2, rt, 15 min; (b) **18** or **23**, 1*H*-tetrazole, CH_2Cl_2, rt, 24 h; (c) *tert*-BuOOH, CH_2Cl_2, rt, 5 min, **26** (22%), **27** (45%), **28** (63%), **29** (11%); (ii) H_2/Pd–C, *t*BuOH–H_2O, 24 h, **2** (34%), **2**′ (35%), **3** (44%), **3**′ (22%).

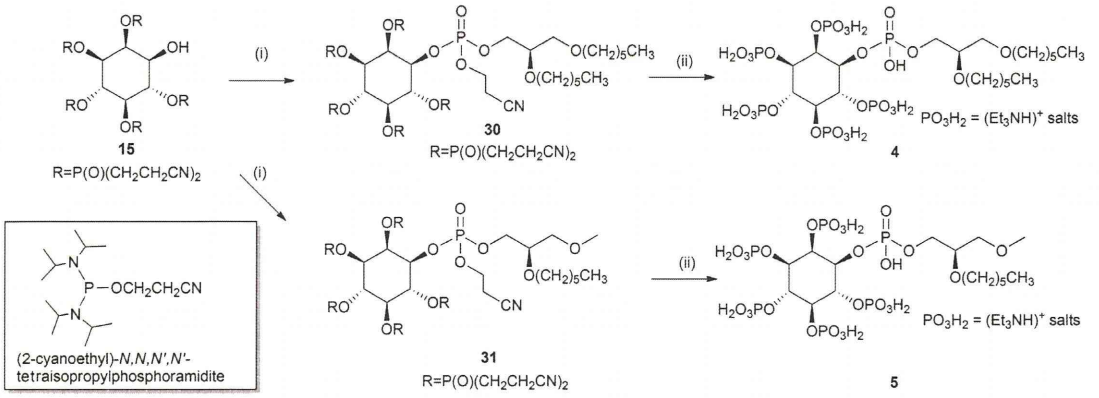

Scheme 6 *Reagents and conditions*: (i) (a) (2-cyanoethyl)-*N,N,N',N'*-tetraisopropylphosphoramidite, 1*H*-tetrazole, CH_2Cl_2, rt, 1.5 h; (b) **20** or **25**, 1*H*-tetrazole, CH_2Cl_2, rt, 2 h; (c) *tert*-BuOOH, CH_2Cl_2, rt, 5 min, **30** (41%) and **31** (63%); (ii) aq. NH_3, MeOH, 55 °C, 10 h, **4** (64%) and **5** (31%).

diacylglycerol moiety interact with MA tightly. The binding affinity of **2′** was 7.60 μM (Fig. 4d), which was 3-fold lower than that of the **3**-MA complex (K_d = 2.04 μM) (Fig. 4f), and almost the same as that of the **2′**-MA complex (K_d = 9.01 μM) (Fig. 4h). These data showed that the phosphate isomers **2′** and **3′** bound MA more weakly than 1-phosphate derivatives **2** and **3**. In contrast, the MA-binding affinity of **4** having an alkyl chain at the glycerol moiety was 1.37 μM (Fig. 4j), which was 18-fold lower than that of the PIP_2 derivative **1**, and was 5-fold higher than that of the diacyl derivative **2** (K_d = 0.25 μM). These data revealed that the diacyl glycerol structure is better than the dialkyl glycerol structure in MA binding. The K_d value for the **5**-MA complex was 7.98 μM (Fig. 4l), which was almost the same as that of **2′** and **3′**-MA complex. In SPR analyses, all PIP_5 derivatives bound MA more tightly than the PIP_2 derivative **1**, IP_6 and IP_3. The order of K_d was **2** < **4** < **3** < **5** = **2′** < **3′** < **1** < IP_6 < IP_3. The structure–activity relationship of these compounds revealed that a highly phosphorylated inositol structure and diacyl (not monoacyl) glycerol at 1-position of inositol are important for MA domain binding.

To confirm the regiochemistry of **2** and **2′**, we synthesized **2** again by an independent route using dibenzyl *N,N*-diethylphosphoramidite that does not cause phosphate migration. In fact, compound **2** was obtained as a sole product without the accompanying isomer **2′**. The newly synthesized **2** showed a K_d value virtually identical to that obtained before (scheme 5), verifying the regiochemistry of **2** (ESI 2†).

2.7. Theoretical binding analysis of MA–1 or MA–2 complexes

A molecular docking study (MOE) was adapted to the **MA–1** and **MA–2** complexes. The structures of complexes around the binding pocket are shown in Fig. 6a and c, and the detailed structures are shown in Fig. 6b and d, wherein lime green lines (ionic interaction) and light blue lines with cylinder solid (H-acceptor) indicate that the interaction between amino acids and **1** (or **2**) is shorter than 4.0 Å, respectively. The surrounded binding pocket of the **MA–1** complex revealed that both inositol and 2′-acyl group of **1** are accommodated in the MA binding pocket. In contrast, the 1′-acyl chain is located outside the binding pocket (Fig. 6a). Although a similar calculated result was obtained for the **MA–2** complex, the outside orientation of the 1′-acyl chain was more pronounced (Fig. 6c). As shown in Fig. 6b, the 1-phosphate interacts with Arg22 (2.9 Å: NH_2, ionic; 3.0, 3.7 Å: NH, H-acceptor). The 4-phosphate interacts with Lys98 (2.6, 2.9, 3.8 Å: NH_2, ionic; 2.6 Å: NH_2, H-acceptor), whereas the 5-phosphate interacts with Arg76 (3.0 Å: NH_2, 2.6, 3.6, 3.9 Å: NH, ionic; 3.0 Å: NH_2, 2.6 Å: NH, H-acceptor). In the case of **2** (Fig. 6d), the 2′-acyl carbonyl oxygen of **2** interacts with Lys27 (2.9 Å: NH_2, H-acceptor). The 1-phosphate interacts with Arg22 (2.8, 3.0 Å: NH_2, 3.5 Å: NH_2, ionic; 3.0, 3.7 Å: NH, H-acceptor). The 2-phosphate interacts with Arg22 (2.6, 3.5 Å: NH_2, ionic; 2.6 Å: NH_2, 3.0 Å: CH_2, H-acceptor). The 3-phosphate interacts with Lys98 (2.7, 2.7 Å: NH_2, ionic; 2.7, 2.7 Å: NH_2, H-acceptor). The 4-phosphate interacts with Lys98 (2.6, 2.8 Å: NH_2, ionic; 2.6, 2.8 Å: NH_2, H-acceptor). The 5-phosphate interacts with Arg76 (2.8 Å: NH_2, 2.6, 3.4 Å: NH, ionic; 2.8 Å: NH_2, 2.6, 3.4 Å: NH, H-acceptor). The **MA–2** complex showed a greater number of amino acid interactions compared with **MA–1**, owing to the greater number of phosphates of **2**. Although 1-, 4-, and 5-phosphate of both **1** and **2** interact with Arg22, Lys98, and Arg76, respectively, 2- and 3-phosphate of **2** additionally interact with Arg22 and Lys98, respectively. In this context, judging from the results of the docking score based on the electric interaction, van der Waals attraction and strain energy of the ligand, the **MA–2** complex was more stable than the **MA–1** complex (−374.7 kcal and −250.2 kcal as the U_dock values, respectively). This is in agreement with SPR data (0.25 μM and 16.9 μM as the K_d values, respectively).

Saad *et al.* demonstrated an "extended lipid" conformation of the **MA–1** complex, in which the glycerol 2′-acyl chain is accommodated in the MA cleft and the glycerol 1′-acyl remains buried in the membrane.[5] Thus, the 1′-acyl does not contribute to MA binding. However, in our study, although the MOE ana-

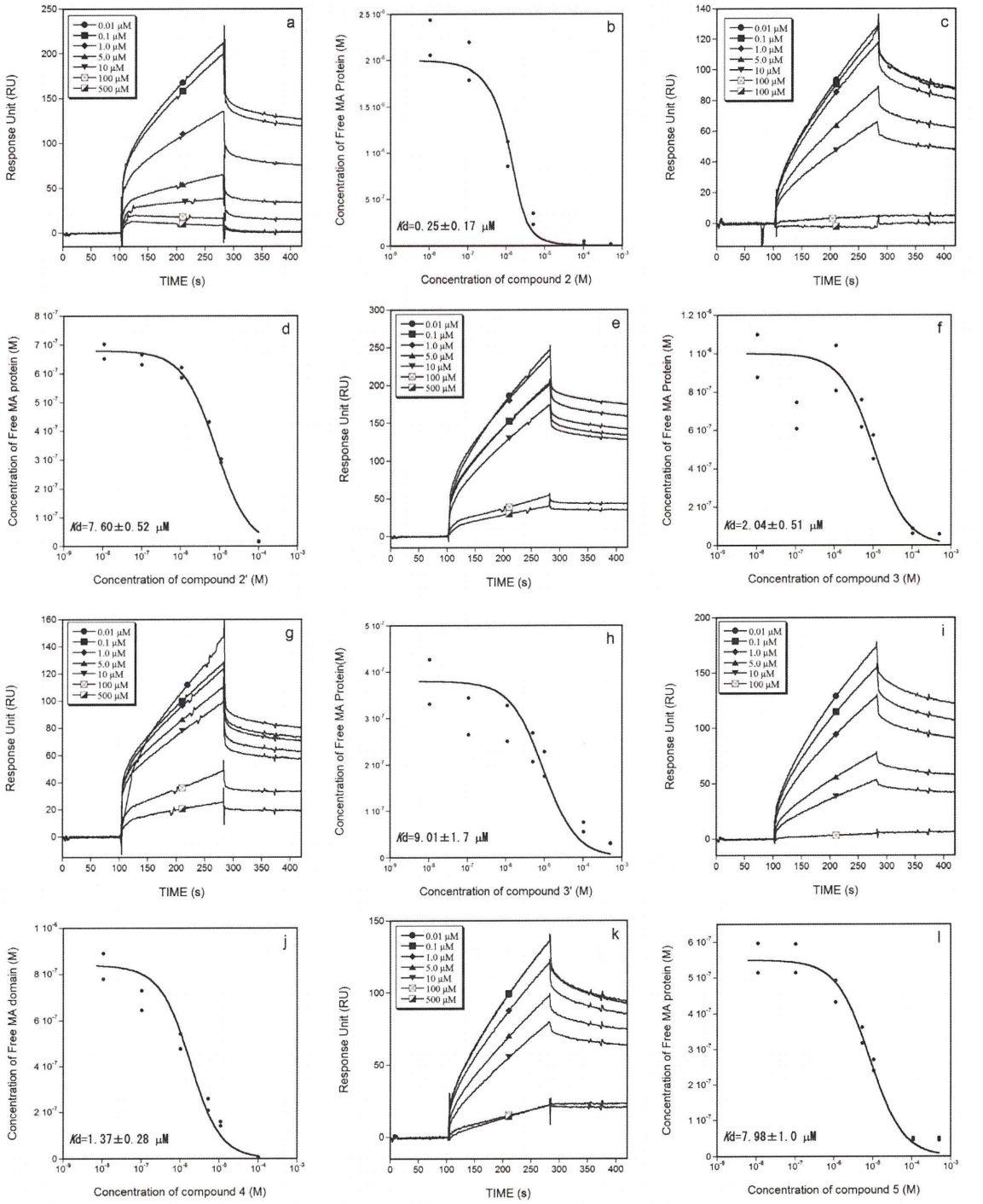

Fig. 4 Competition assay and calculation of the equilibrium dissociation constants (K_d) for MA-competitor complexes. The sensorgrams of MA and competitors, **2** (a), **2'** (c), **3** (e), **3'** (g), **4** (i), and **5** (k) are shown. The competition curves between uncompetitive MA and **2** (b), **2'** (d), **3** (f), **3'** (h), **4** (j), and **5** (l) are shown. Calculated K_d values are shown. Each experiment was performed in duplicate.

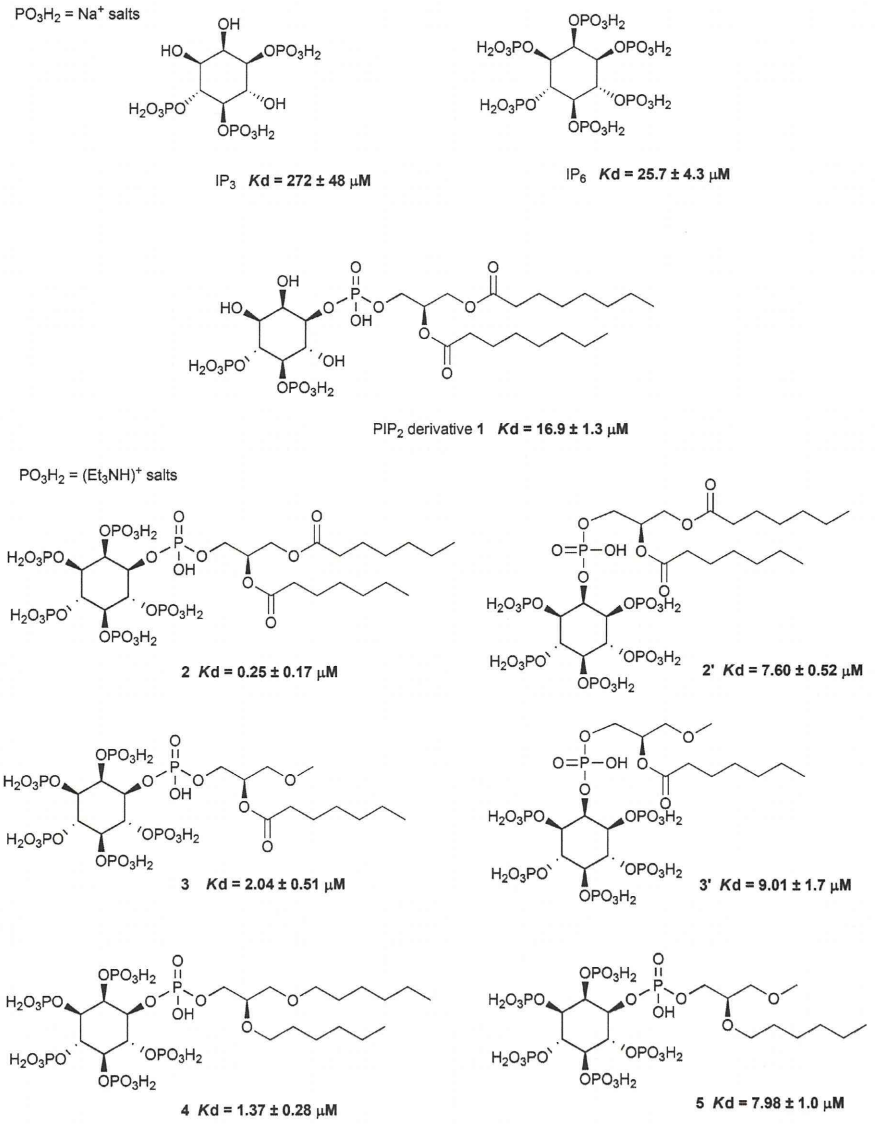

Fig. 5 Dissociation constant (K_d) of MA complexed with IPs, PI, and PIP_5 derivatives.

lysis of the MA–**2** complex indicates that the 1′-acyl was located outside the binding pocket, **3** (without the 1′-acyl) did not bind MA (K_d = 2.04 μM) as strongly as **2** (K_d = 0.25 μM) did, as revealed by the SPR analysis. It is hypothesized that the difference of K_d values between **3** and **2** is caused not only by the interaction between the 2′-acyl chain and hydrophobic region of MA but also by the interaction between primordial carbons of the 1′-acyl chain of **2** and the hydrophobic region of MA, which was not observed in MOE analysis.

Freed *et al.*[2,21] demonstrated the role of the MA in the HIV-1 replication and mapped the functional domains within this protein by site-directed mutagenesis to introduce over 80 single amino acid substitutions into MA and analyzed the effects on a variety of aspects of virus life cycles. They observed that a single amino acid mutation near the terminus of MA and in the vicinity of residues 55 and 85 caused virus assembly defects. Furthermore, they identified that a highly basic domain between MA residues 17 and 31 (16 and 30 in the MOE number) is implicated in membrane binding. In this MOE analysis, not only Arg22 at a highly basic region but also the amino acids which have never been investigated, Arg76 and Lys98, are implicated in MA–**1** binding.

HIV-1 is a retrovirus, which is a family of enveloped viruses that replicate in a host cell through the process of reverse tran-

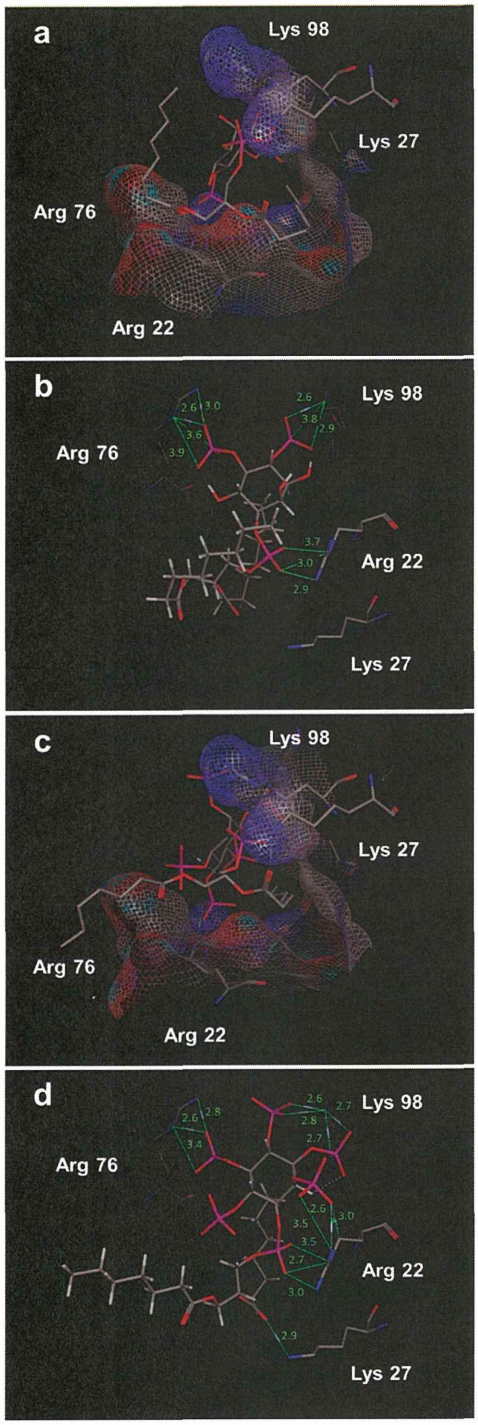

Fig. 6 Docking studies of MA–**1** (a, b) and MA–**2** (c, d) complexes. The lime green lines (ionic interaction) and light blue lines with cylinder solid (H-acceptor) indicate the interaction between amino acids and **1** (b) or **2** (d) shorter than 4.0 Å, respectively.

scription. Retroviruses have Gag, Pol, and Env proteins. Chan *et al.*[22] examined the possible role of PIP_2 in Gag-membrane interaction of the alpharetrovirus Rous sarcoma virus (RSV) and showed that neither membrane localization of RSV Gag-GFP nor release of virus-like particles was affected by phosphatase-mediated depletion of PIP_2 in transfected avian cells. Furthermore, Inlora *et al.*[23] determined the role of the MA–PIP_2 interaction in Gag localization and membrane binding of a deltaretrovirus, human T-lymphotropic virus type 1 (HTLV-1). They demonstrated that, unlike HIV-1 Gag, subcellular localization of Gag and virus-like particles released by HTLV-1 was minimally sensitive to polyphosphoinositide 5-phosphatase IV (5ptaseIV) overexpression. These results suggest that the interaction of HTLV-1 MA with PIP_2 is not essential for HTLV-1 particle assembly. Accordingly, MA–PIP_2 binding might be significant only in HIV-1 among retroviruses, and our findings of MA-binding of PIP_5 derivatives may be HIV-1 specific.

Although PIP_5 derivatives bind MA tightly, when highly charged these derivatives would not permeabilize the cell membrane in spite of the fact that the viral assembly occurs inside the cell. We intend to use a membrane carrier or synthesize a phosphate prodrug compound to improve the cell membrane permeability in the future.

3. Materials and methods

3.1. General methods

Chemicals were purchased from Aldrich, Fluka, Kanto Chemical, Nacalai tesque, and Wako. Thin layer chromatography (TLC) was performed on precoated plates (Merck TLC sheets silica 60 F_{254}): products were visualized by spraying phosphomolybdic acid in EtOH or basic potassium permanganate and heated at high temperature. Chromatography was carried out on Silica Gel 60 N (40–100 mesh). Reverse phase chromatography was performed using a C_{18} column (Cole-Parmer, USA). Cation exchange chromatography was performed using Dowex 50WX8 (H^+, 100–200 mesh). NMR spectra (JEOL JNM-AL300) were referenced to $SiMe_4$ or HDO. Infra-red spectra were recorded on a JASCO FT/IR-410. The samples were prepared as KBr discs or thin films between sodium chloride discs. Microanalysis was carried out using a Yanaco MT-5S. High resolution MS (HRMS) were recorded with a JEOL JMS-DX303HF by using positive and negative FAB with 3-nitrobenzyl alcohol (NBA) (containing HMPA or not) as the matrix.

3.2. DL-3,6-Di-*O*-benzyl-1,2:4,5-di-*O*-cyclohexylidene-*myo*-inositol (7)

To a solution of DL-1,2:4,5-di-cyclohexylidene-*myo*-inositol **6** (2.27 g, 6.67 mmol) in DMF (10 ml) was added NaH (0.676 g, 28.1 mmol) followed by benzyl bromide (2.0 ml, 16.9 mmol), and the resulting mixture was stirred at room temperature under argon for 24 h. The reaction was quenched with MeOH, and concentrated under reduced pressure, and the residue was diluted with AcOEt. The organic phase was washed with H_2O and saturated aqueous NaCl, dried over Na_2SO_4, and then

concentrated under reduced pressure. The crude product was purified by silica gel column chromatography (hexane–AcOEt = 5 : 1) to afford 7 (3.25 g, 94%) as a white solid.

^{1}H NMR ($CDCl_3$) δ: 1.25–1.69 (20H, m, $CH_2 \times 10$), 3.33 (1H, t, J = 9.3 Hz, C*H*), 3.62–3.67 (1H, dd, J = 10.6, 6.6 Hz, C*H*), 3.71–3.76 (1H, dd, J = 4.2, 10.2 Hz, C*H*), 3.98 (1H, d, J = 9.7 Hz, C*H*), 4.02–4.06 (1H, d, J = 5.1, 6.4 Hz, C*H*), 4.33 (1H, t, J = 4.5 Hz, C*H*), 4.78–4.90 (4H, m, $CH_2 \times 2$), 7.22–7.43 (10H, m, $C_6H_5 \times 2$). ^{13}C NMR ($CDCl_3$) δ: 23.9, 24.2, 24.3, 24.4, 25.4, 25.5, 35.7, 36.9, 37.8, 72.0, 72.3, 75.0, 76.6, 77.2, 79.1, 80.3, 81.0, 110.8, 113.1, 127.8, 128.1, 128.4, 128.5, 128.6, 128.7, 138.5, 138.7. IR (KBr) 3030, 2935, 2860, 1500, 1165, 1110, 850, 830, 740 cm^{-1}. MS (FAB) m/z 521 $(M + H)^+$. Mp. 123 °C. Anal. Calcd for $C_{32}H_{40}O_6$: C, 73.82; H, 7.74. Found: C, 73.87; H, 7.98. TLC; R_f 0.42 (hexane–AcOEt = 5 : 1).

3.3. DL-3,6-Di-*O*-benzyl-*myo*-inositol (8)

To a solution of 7 (3.95 g, 7.58 mmol) in THF–H_2O (5 : 1, 60 ml) was added *p*-toluenesulfonic acid monohydrate (1.90 g, 10.0 mmol). The resulting mixture was refluxed for 5 h, and then neutralized with Et_3N, and concentrated under reduced pressure. The crude product was washed with a heated AcOEt, and the resulting crystals were filtered. Drying the crystal under reduced pressure afforded **8** (2.22 g, 81%) as a white solid.

^{1}H NMR (DMSO) δ: 2.49 (3H, bs, O*H* × 3), 3.12 (2H, t, J = 9.9 Hz, C*H* × 2), 3.28 (1H, d, J = 7.3 Hz, C*H*), 3.59 (2H, t, J = 9.5 Hz, C*H* × 2), 3.95 (1H, s, C*H*), 4.53–4.79 (4H, m, CH_2), 7.21–7.42 (10H, m, $C_6H_5 \times 2$). ^{13}C NMR ($CDCl_3$) δ: 69.8, 70.8, 71.4, 72.3, 73.4, 75.0, 79.8, 81.8, 126.9, 127.1, 127.5, 127.8, 128.0, 139.3, 139.9. IR (KBr) 3750, 3030, 2905, 1500, 1450, 1110, 900, 740 cm^{-1}. Mp. 204 °C. MS (FAB) m/z 383 $(M + Na)^+$. Anal. Calcd for $C_{20}H_{24}O_6$: C, 66.65; H, 6.71. Found: C, 66.40; H, 6.83. TLC; R_f 0.48 (CH_2Cl_2–MeOH = 7 : 1).

3.4. DL-3,6-Di-*O*-benzyl-1-*O*-(*p*-methoxybenzyl)-*myo*-inositol (9)

A mixture of **8** (2.10 g, 5.66 mmol) and dibutyltin oxide (1.74 g, 7.00 mmol) in toluene (100 ml) was refluxed for 3 h in a Dean–Stark apparatus to remove water. The mixture was concentrated under reduced pressure. To the residue was added cesium fluoride (1.06 g, 7.00 mmol), and the mixture was suspended in heated DMF (30 ml) at 100 °C. To the resulting suspension was added *p*-methoxybenzyl chloride (0.887 ml, 6.20 mmol) at −78 °C, and the mixture was stirred at room temperature under argon for 48 h. After concentration of the reaction mixture under reduced pressure, the residue was purified by silica gel column chromatography (CH_2Cl_2–MeOH = 10 : 1) to afford **9** (2.40 g, 89%) as a white solid.

^{1}H NMR ($CDCl_3$) δ: 2.48 (1H, bs, O*H*), 2.65 (2H, bs, O*H*), 3.19–3.23 (1H, dd, J = 2.7, 9.5 Hz, C*H*), 3.39 (1H, t, J = 9.3 Hz, C*H*), 3.76–3.82 (4H, m, OCH_3, C*H*), 3.95 (1H, t, J = 9.3 Hz, C*H*), 4.16 (1H, s, C*H*), 4.61–4.70 (4H, m, $CH_2 \times 2$), 4.75 (1H, d, J = 11.2 Hz, $C_6H_5CH_2$(C*H*)), 4.93 (1H, d, J = 11.2 Hz, $C_6H_5CH_2$(C*H*)), 6.85 (2H, d, J = 8.8 Hz, $CH_3OC_6H_4$(C*H* × 2)), 7.23–7.36 (12H, m, $C_6H_5 \times 2$, $CH_3OC_6H_5$(C*H* × 2)). ^{13}C NMR ($CDCl_3$) δ: 55.2, 67.0, 71.9, 72.0, 72.2, 74.2, 75.3, 79.0, 79.4, 80.4, 113.8, 127.6, 127.9, 127.9, 128.4, 128.5, 129.5, 129.9, 137.8, 137.9, 138.7, 159.4, 162.5. IR (KBr) 3460, 2880, 1610, 1520, 1450, 1180, 1100, 810, 750 cm^{-1}. Mp. 154 °C. MS (FAB) m/z 503 $(M + Na)^+$. Anal. Calcd for $C_{28}H_{32}O_7$: C, 69.98; H, 6.71. Found: C, 70.02; H, 6.76. TLC; R_f 0.50 (CH_2Cl_2–MeOH = 10 : 1).

3.5. DL-1-*O*-(*p*-Methoxybenzyl)-*myo*-inositol (10)

To a solution of **9** (1.86 g, 3.87 mmol) in MeOH (25 ml) was added W-2 RANEY® Nickel (0.20 g, 3.03 mmol), and the resulting mixture was stirred at 50 °C under hydrogen for 3 h. The mixture was filtered through a pad of celite and concentrated under reduced pressure. The residue was washed with heated AcOEt, and the resulting crystals were filtered. Drying of the crystals under reduced pressure afforded **10** (0.52 g, 45%) as a white solid.

^{1}H NMR (DMSO) δ: 2.91–2.94 (1H, m, C*H*), 3.03–3.06 (2H, m, C*H*), 3.33–3.36 (1H, m, C*H*), 3.48–3.52 (1H, m, C*H*), 3.73 (3H, s, C*H*), 3.91 (1H, s, C*H*), 4.36–4.57 (7H, m, O*H* × 5, CH_2), 6.87 (2H, d, J = 8.8 Hz, $CH_3OC_6H_5$(C*H* × 2)), 7.31 (2H, d, J = 8.4 Hz, $CH_3OC_6H_5$(C*H* × 2)). ^{13}C NMR (DMSO) δ: 55.0, 69.3, 70.3, 71.7, 72.0, 72.4, 75.4, 79.6, 113.4, 129.0, 131.2, 158.5. IR (KBr) 3390, 2910, 1610, 1590, 1510, 1250, 1120, 890, 820 cm^{-1}. Mp. 183 °C. MS (FAB) m/z 299 $(M - H)^+$. Anal. Calcd for $C_{14}H_{20}O_7$: C, 55.99; H, 6.71. Found: C, 56.06; H, 6.72. TLC; R_f 0.39 (CH_2Cl_2–MeOH = 3 : 1).

3.6. DL-1-*O*-(*p*-Methoxybenzyl)-2,3,4,5,6-penta-*O*-[(1,5-dihydro-2,4,3-benzodioxaphosphepin-3-yl)phosphoryl]-*myo*-inositol (11)

To a suspension of **10** (0.050 g, 0.166 mmol) in CH_2Cl_2 (10 ml) was added MS4A, and the resulting suspension was stirred at room temperature under argon for 15 min. To the mixture was added (1,5-dihydro-2,4,3-benzodioxaphosphepin-3-yl)diethylamine (0.358 ml, 1.66 mmol) followed by 1*H*-tetrazole (0.116 g, 1.66 mmol), the resulting mixture was stirred overnight at room temperature under argon. To the mixture was added *m*-chloroperbenzoic acid (0.336 g, 1.50 mmol) in small portions, and the resulting mixture was stirred at −40 °C to room temperature for 1 hour. The mixture was purified by silica gel column chromatography (AcOEt–hexane = 15 : 1) to afford **11** (0.151 g, 75%) as a white yellow solid.

^{1}H NMR ($CDCl_3$) δ: 3.82 (3H, s, OCH_3), 3.92 (1H, d, J = 8.6 Hz, C*H*), 4.52 (1H, d, J = 10.4 Hz, C*H*), 4.72–5.80 (26H, m, CH_2, $C_6H_4(CH_2)_2 \times 5$, C*H* × 4), 6.90 (2H, d, J = 8.4 Hz, $CH_3OC_6H_4$(C*H* × 2)), 6.96 (20H, m, $C_6H_4 \times 5$), 7.46 (2H, d, J = 8.4 Hz, $CH_3OC_6H_4$(C*H* × 2)). ^{13}C NMR ($CDCl_3$) δ: 55.1, 68.0, 68.9, 69.2, 74.4, 75.4, 76.6, 77.0, 77.2, 77.4, 113.5, 128.4, 128.5, 128.6, 128.7, 128.8, 128.8, 129.0, 129.0, 129.2, 129.4, 129.8, 134.3, 135.1, 135.2, 135.5, 135.6, 159.1. IR (KBr) 1610, 1510, 1460, 1380, 1290, 1020, 860, 730 cm^{-1}. Mp 165 °C. HRMS(FAB) m/z calcd for $C_{54}H_{56}O_{22}P_5$ $(M + H)^+$ 1211.2022. Found: 1211.1870. Anal. Calcd for $C_{54}H_{56}O_{22}P_5$: C, 53.56; H, 4.58. Found: C, 53.21; H, 4.72. TLC; R_f 0.55 (CH_2Cl_2–MeOH = 10 : 1).

3.7. DL-2,3,4,5,6-Penta-*O*-[(1,5-dihydro-2,4,3-benzodioxaphosphepin-3-yl)phosphoryl]-*myo*-inositol (12) and DL-1,3,4,5,6-penta-*O*-[(1,5-dihydro-2,4,3-benzodioxaphosphepin-3-yl)phosphoryl]-*myo*-inositol (13)

To a solution of **11** (0.070 g, 0.0578 mmol) in CH_3CN–H_2O (9 : 1, 5 ml) was added diammonium cerium(IV) nitrate (0.158 g, 0.288 mmol) and the resulting mixture was stirred at room temperature for 1 hour. The mixture was concentrated under reduced pressure, and the residue was purified by silica gel column chromatography (CH_2Cl_2–MeOH = 10 : 1) to afford the mixture of **12** and **13**. Compounds **12** and **13** were used for the next coupling reaction without further purification.

R_f values of compounds **12** and **13** were 0.37 and 0.29, respectively (CH_2Cl_2–MeOH = 10 : 1).

3.8. DL-1-*O*-(*p*-Methoxybenzyl)-2,3,4,5,6-penta-*O*-[bis(2-cyanoethyl)phosphoryl]-*myo*-inositol (14)

To a suspension of **10** (0.050 g, 0.166 mmol) in CH_2Cl_2 (10 ml) was added MS4A, and the resulting suspension was stirred at room temperature under argon for 15 min. To the mixture was added bis(2-cyanoethyl)-*N*,*N*-diisopropylphosphoramidite (0.383 ml, 1.50 mmol) followed by 1*H*-tetrazole (0.105 g, 1.50 mmol), the resulting mixture was stirred at room temperature under argon for 4 h. To the mixture was added *m*-chloroperbenzoic acid (0.336 g, 1.50 mmol) in small portions, and the resulting mixture was stirred at −78 °C to room temperature for 1 hour. The mixture was purified by silica gel column chromatography (CH_2Cl_2–MeOH = 7 : 1) to afford **14** (0.15 g, 73%) as a colorless oil.

^{1}H NMR (CD_3COCD_3) δ: 2.65–2.91 (20H, m, CH_2CH_2CN × 10), 3.68 (3H, s, OCH_3), 3.95 (1H, d, J = 9.3 Hz, C*H*), 4.11–4.51 (21H, m, CH_2CH_2CN × 10, C*H*), 4.65–4.80 (5H, m, CH_2, C*H* × 3), 5.36 (1H, d, J = 9.2 Hz, C*H*), 6.84 (2H, d, J = 8.8 Hz, $CH_3OC_6H_5$(C*H* × 2)), 7.39 (2H, d, J = 8.63 Hz, $CH_3OC_6H_5$(C*H* × 2)). IR (KBr) 3300, 2890, 2255, 1610, 1470, 1415, 1280, 1040, 820, 795, 765 cm^{-1}. HRMS(FAB) *m*/*z* calcd for $C_{44}H_{55}N_{10}O_{22}P_5$ $(M + Na)^+$ 1253.2078. Found: 1253.2029. TLC; R_f 0.28 (CH_2Cl_2–MeOH = 10 : 1).

3.9. DL-2,3,4,5,6-Penta-*O*-[bis(2-cyanoethyl)phosphoryl]-*myo*-inositol (15)

To a solution of **14** (0.073 g, 0.059 mmol) in CH_3CN–H_2O (9 : 1, 10 ml) was added diammonium cerium(IV) nitrate (0.208 g, 0.379 mmol) and the resulting mixture was stirred at room temperature for 1.5 h. The mixture was concentrated under reduced pressure, and the residue was purified by silica gel column chromatography (CH_2Cl_2–MeOH = 7 : 1 to 3 : 1) to afford **15** (0.055 g, 68%) as a colorless oil.

^{1}H NMR (CD_3COCD_3 + D_2O) δ: 2.93–3.02 (20H, m, CH_2CH_2CN × 10), 4.22 (1H, s, C*H*), 4.41–4.53 (20H, m, CH_2CH_2CN × 10), 4.64–4.94 (4H, m, C*H* × 4), 5.20 (1H, d, J = 9.0 Hz, C*H*). ^{13}C NMR (CD_3COCD_3) δ: 19.8, 19.9, 19.9, 20.0, 20.0, 63.9, 64.0, 64.1, 64.2, 64.3, 64.3, 64.6, 68.8, 74.5, 76.1, 76.8, 79.0, 79.2, 79.2, 118.3, 118.4, 118.6. IR (film) 3020, 2910, 2255, 1635, 1470, 1415, 1340, 1280, 1040 cm^{-1}. HRMS(FAB) *m*/*z* calcd for $C_{36}H_{47}N_{10}O_{21}P_5$ $(M + Na)^+$ 1133.1503. Found: 1133.1545. R_f 0.25 (CH_2Cl_2–MeOH = 7 : 1).

3.10. (*R*)-1-Benzyloxy-2,3-bis(heptanoyl)propane (17)

To a mixture of (*R*)-3-benzyloxy-1,2-propandiol (**16**) (0.10 g, 0.549 mmol) in CH_2Cl_2 (5 ml) was added pyridine (0.11 ml, 1.37 mmol) followed by dimethylaminopyridine (0.0036 g, 0.27 mmol) and the resulting mixture was cooled to 0 °C. To the mixture was added heptanoyl chloride (0.20 ml, 1.26 mmol) and the resulting mixture was stirred overnight at room temperature under argon. The reaction was quenched with H_2O (25 ml), and the resulting water phase was extracted with CH_2Cl_2. The organic layer was washed with 2 M aqueous hydrogen chloride (20 ml) and H_2O (25 ml). The resulting organic phase was further washed with brine (30 ml) and dried over Na_2SO_4, and then concentrated under reduced pressure. The crude product was purified by silica gel column chromatography (hexane–AcOEt = 9 : 1) to afford **17** (0.193 g, 86%) as a colorless oil.

^{1}H NMR ($CDCl_3$) δ: 0.86–0.90 (6H, m, CH_3 × 2), 1.28–1.36 (12H, m, CH_2 × 6), 1.54–1.66 (4H, m, CH_2 × 2), 2.25–2.34 (4H, m, CH_2 × 2), 3.59 (2H, d, J = 5.1 Hz, $CH_2OCH_2C_6H_5$), 4.15–4.22 (1H, dd, J = 6.2, 11.7 Hz, CH_2OCO), 4.32–4.37 (1H, dd, J = 3.8, 11.9 Hz, CH_2OCO), 4.49–4.58 (2H, dd, J = 12.1, 15.2 Hz, $C_6H_5CH_2$), 5.20–5.27 (1H, ddt, J = 3.9, 5.1, 6.2 Hz, CH_2CHCH_2), 7.26–7.37 (5H, m, C_6H_5). ^{13}C NMR ($CDCl_3$) δ: 14.0, 22.4, 24.8, 24.9, 28.7, 28.8, 31.4, 34.1, 34.3, 62.6, 68.3, 70.0, 73.3, 127.6, 127.7, 128.4, 137.7, 173.1, 173.4. IR (KBr) 2820, 1740, 1460, 1160, 1100, 740, 700 cm^{-1}. HRMS(FAB) *m*/*z* calcd for $C_{24}H_{39}O_5$ $(M + H)^+$ 407.2797. Found: 407.2760. Anal. Calcd for $C_{24}H_{39}O_5$: C, 70.90; H, 9.42. Found: C, 70.61; H, 9.62. TLC; R_f 0.35 (hexane–AcOEt = 9 : 1).

3.11. 1,2-*O*-Diheptanoyl-*sn*-glycerol (18)

To a solution of **17** (0.193 g, 0.475 mmol) in CH_2Cl_2 (10 ml) was added 10% Pd–C (0.126 g, 0.119 mmol), and the resulting mixture was stirred overnight at room temperature under hydrogen. The mixture was filtered through a pad of celite, and the resulting filtrate was concentrated under reduced pressure. The crude product was purified by silica gel column chromatography (hexane–AcOEt = 2 : 1) to afford **18** (0.144 g, 96%) as a colorless oil.

^{1}H NMR ($CDCl_3$) δ: 0.89 (6H, t, J = 6.8 Hz, CH_3 × 2), 1.21–1.37 (12H, m, CH_2 × 6), 1.50–1.68 (4H, m, CH_2 × 2), 2.12 (1H, bs, O*H*), 2.30–2.37 (4H, dd, J = 7.1, 14.5 Hz, CH_2 × 2), 3.38 (2H, bs, $HOCH_2$), 4.20–4.26 (1H, dd, J = 5.7, 11.9 Hz, OCOC*H*H), 4.30–4.35 (1H, dd, J = 4.6, 11.9 Hz, OCOCH*H*), 5.00–5.12 (1H, m, C*H*). ^{13}C NMR ($CDCl_3$) δ: 14.0, 22.4, 22.5, 24.8, 24.9, 28.7, 28.8, 31.4, 34.1, 34.3, 61.5, 62.0, 173.4, 173.6. IR (KBr) 3590, 3140, 2930, 2860, 1740, 1160, 1100 cm^{-1}. HRMS (FAB) *m*/*z* calcd for $C_{17}H_{32}O_5$ $(M + Na)^+$ 339.2147. Found: 339.2154. Anal. Calcd for $C_{17}H_{32}O_5$: C, 64.53; H, 10.19. Found: C, 64.33; H, 10.22. TLC; R_f 0.45 (hexane–AcOEt = 2 : 1).